CHAPTER FOUR

Selected polyazole based coordination polymers displaying functional properties

Yann Garcia*
Institute of Condensed Matter and Nanosciences, Molecular Chemistry, Materials and Catalysis Division (IMCN/MOST), Université catholique de Louvain, Louvain-La-Neuve, Belgium
*Corresponding author: e-mail address: yann.garcia@uclouvain.be

Contents

Abstract

In this account, we present recent on-going developments on the design and synthesis of transition metal (M(II) = Fe, Cu, Zn, Cd, Hg) coordination networks built from 1,2,4-triazole, tetrazole, benzimidazole or pyrazole building blocks. Special focus is placed on the use of a high energetic material made of a dissymmetric 1,2,4-triazole-tetrazole ligand, able to provide coordination polymers of alkali metals and alkaline earth metals, as well as salts. These materials, apart from their structural diversity and appeal, present some potential applications in gas or metallic storage, molecular electronics (spin cross-over), gas sensing, toxic metal sensing and capture, as well as in medicinal applications.

1. Introduction

Ligand molecules containing azole building blocks are widely used as organic connectors in supramolecular coordination chemistry,[1] as an alternative to classic pyridine and other nitrogen donor molecules.[2] Such molecules, which are often coordinated in multi-dentate fashion, have afforded a

Advances in Inorganic Chemistry, Volume 76
ISSN 0898-8838
https://doi.org/10.1016/bs.adioch.2020.04.001

variety of metal organic frameworks (MOFs) and coordination polymers (CPs) of different topologies. Such networks range from one dimensional (1D) CPs to two dimensional (2D) layered or three dimensional (3D) metal-azolate/azole networks (MANs).[3] Numerous functional properties were discovered with applications in gas storage,[4] catalysis,[5] chromatography,[6] optics,[7] magnetism,[8] health,[9] to name but a few. Among azole networks, those with 1,2,4-triazole or tetrazole building blocks coordinated to Fe(II) ions have attracted special interest because of their ligand field strength, which was found to be in the expected range for thermally induced spin crossover (SCO) observation.[10] For instance, the Fe(II) CP $[Fe(btzp)_3](ClO_4)_2$ (**1**) (***btzp*** = 1,4-bis (tetrazol-1-yl)butane, Scheme 1) discovered by van Koningsbruggen *et al.*[11] displayed on cooling a reversible SCO behavior, which was the first 1D chain for which the crystal structure was solved, in both low-spin (LS) and high-spin (HS) states. This linear chain allowed to introduce for the first time, the concept of elastic interactions cushioning (so called "airbag" effect) to explain the gradual character of its SCO behavior. In addition, it is considered as the first example of Light Induced Excited Spin State Trapping (LIESST) for a 1D chain, after green light irradiation at liquid helium temperatures.[11]

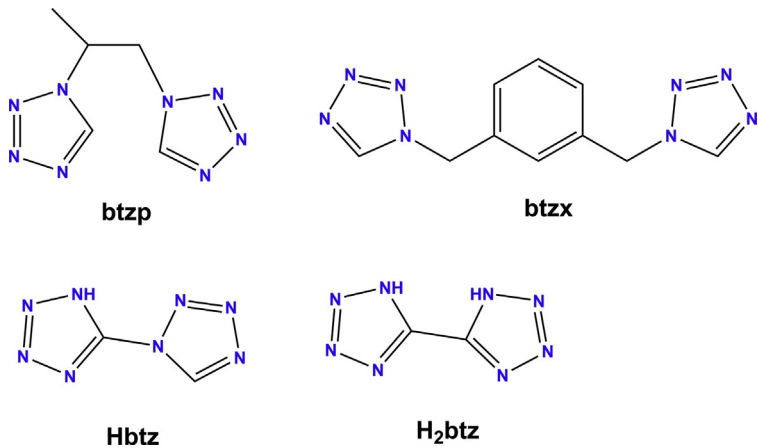

Scheme 1 Molecular structures of selected bis-tetrazole ligands.

Later a number of bis-tetrazole and tris-tetrazole CPs, with different dimensionalities, were investigated,[10,12] some being for instance studied for their gas storage properties, i.e., $[Fe(\mathbf{btzx})_3](ClO_4)_2$ (**2**) (***btzx*** = 1,4-bis (tetrazol-1-ylmethyl)benzene, Scheme 1).[13]

A noticeable interest has been devoted too to 1D Fe(II) chains with 4R-1,2,4-triazole ligands (R = substituent, Scheme 2), due to their synthetic modularity and high yield, allowing to derive structure-magnetic property relationships. Several chemical parameters were varied such as the nature of the R group on the 1,2,4-triazole unit, the counter anions (playing with their size, geometry, charge and volume) and solvent molecules, if any, allowing to discover a wide range of SCO behavior.[14] For instance, a linear relationship was established for the families $[Fe(hyetrz)_3](Anion)_2$ (**3**) (***hyetrz*** = 4–2′-hydroxy-ethyl-1,2,4-triazole),[15] and $[Fe(NH_2trz)_3](Anion)_2$ (**4**) (***NH₂trz*** = 4-amino-1,2,4-triazole),[16] involving the transition temperature observation and the volume of the inserted counter anion. The smaller the volume of the anion, the higher the transition temperature.[17] This has led to the discovery of SCO behavior

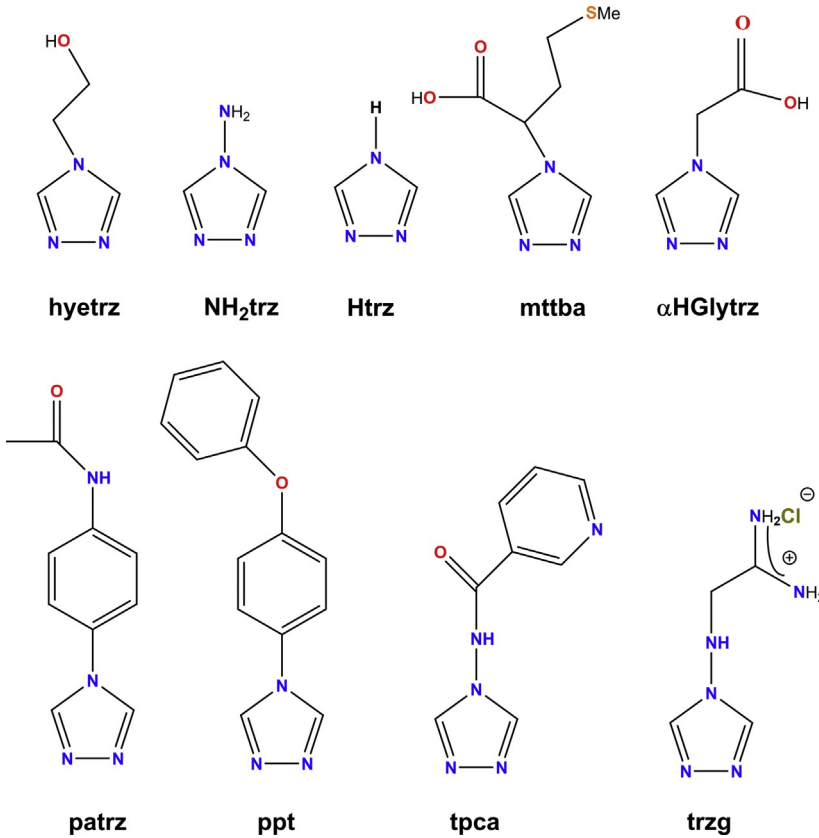

Scheme 2 Molecular structures of selected 4R-1,2,4-triazole molecules (R = substituent).

occurring around the room temperature region, with remarkable themochromic properties, e.g., for $[Fe(hyetrz)_3]I_2$•xsolv (**5**).[15] This material was shown to display, in addition to its thermochromism, weak pressure piezochromism properties allowing to derive a contact pressure optical sensor operating at room temperature. Applications in aeronautics and civil security were for instance proposed.[18] Numerous efforts were also devoted to nano-structuration of these 1D materials as nanoparticles or thin films,[19] while their implementation into spintronic devices has recently been investigated.[20] Hybrid materials including such 1D chains were also prepared, e.g., $[Fe(Htrz)trz]BF_4$ (**6**) (***Htrz*** = 4H-1,2,4-triazole, ***trz*** = 1,2,4-triazolato), embedded into the pores of MCM-41.[21] This material displays exceptional SCO characteristics near the room temperature region, with sharp spin transitions, a reproducible and large thermal hysteresis loop (35 K), as well as a contrasting color change. Last but not least, it does not contain any lattice solvent molecules, which are known to lead to non-reproducible spin transitions and fake hysteresis loops, when removed from the material by heating.

Apart for linear chains, whose polymerization relies on the bidentate mode of 4R-1,2,4-triazole, the design of a higher dimensionality network has involved the use of bis-1,2,4-triazole type ligands containing "long" flexible spacers, after the discovery of the first 2D SCO network, $[Fe(btr)_2(NCS)_2]$•H_2O (**7**) (***btr*** = 4,4′-bis-1,2,4-triazole),[22] and the first 3D SCO network $[Fe(btr)_3](ClO_4)_2$ (**8**).[23] The number of coordination networks with bis-1,2,4-triazole-derivatives remain, however, scarce.[10] This situation presumably depends on synthetic issues associated with the preparation of 4R-triazole precursors, which usually relies on the application of the Bayer's patent synthetic route, which is known to be moderately efficient in terms of yield and often involves unwanted chromatographic work ups.[24] As a result of the desire to efficiently produce 4R-triazole derivatives, and in particular the celebrated ***btr*** and ***btre*** (1,2-bis(1,2,4-triazol-4-yl)ethane) precursors in a large amount (Scheme 3) compared to the multi-step synthetic method from Bartlett and Humphrey,[25] we have revised a classic transamination reaction. This method has been extended to the synthesis of a wide range of 4R-1,2,4-triazole,[26] e.g., ***patrz*** = *N*-(4-(4*H*-1,2,4-triazol-4-yl)phenyl)acetamide (Scheme 2), an active intermediate in the "sumatriptan" drug. This methodology has been adopted by many groups to produce interesting CPs and MOFs.[27] In particular, we have prepared a new range of building blocks based on amino acids, which produced new azole CPs and MOFs.[28,29] In the present chapter, we present selected recent results in crystal engineering of CPs with azole based ligands with interesting properties.

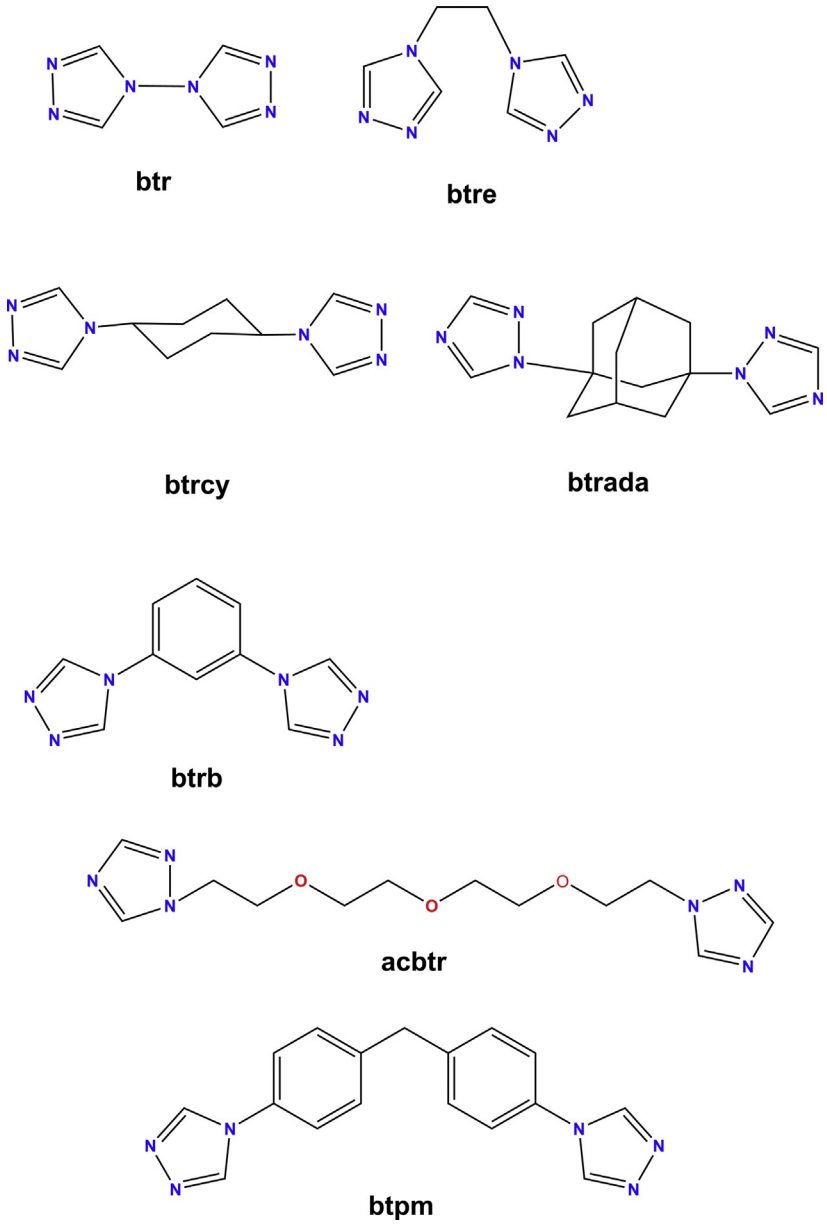

Scheme 3 Molecular structures of selected bis-1,2,4-triazole ligands.

2. Selected coordination networks for metal capture

Maintaining our efforts to produce CPs based on amino acid 1,2,4-triazole derivatives, which were reviewed in 2011,[29] Naik *et al.* have prepared a conformationally flexible triazole-carboxylic acid ligand derived from L-amino acid, namely 4H-1,2,4-triazol-4-yl-acetic acid (**αHGlytrz,** Scheme 2).[28a] Self-assembly of this small molecule in water with $CuSiF_6$ yielded a novel single-wall metal organic nanotube (SWMONT) crystallizing in the P31c space group (Fig. 1). This material of formula $\{[Cu_3(\mu_3\text{-}OH)(H_2O)_3(Glytrz)_3]\cdot SiF_6\cdot 8H_2O\cdot X\}$ (**9**) (where X = disordered lattice water molecules), is made of trinuclear Cu^{II} cluster units.[30] The originality of this material stems from its nano-tubular architecture, which is commonly available in single-walled carbon nanotubes (SWCNTs),[31] but herein prepared by a one-step synthesis using a simple and small organic precursor reacting to a common Cu(II) salt in water (Fig. 1). This material does not suffer any oxidation and could be prepared in diverse forms: (i) as single crystals which allowed to determine its crystal structure by X-ray diffraction. (ii) As powders, on a much larger scale, after checking that its formulation and crystal

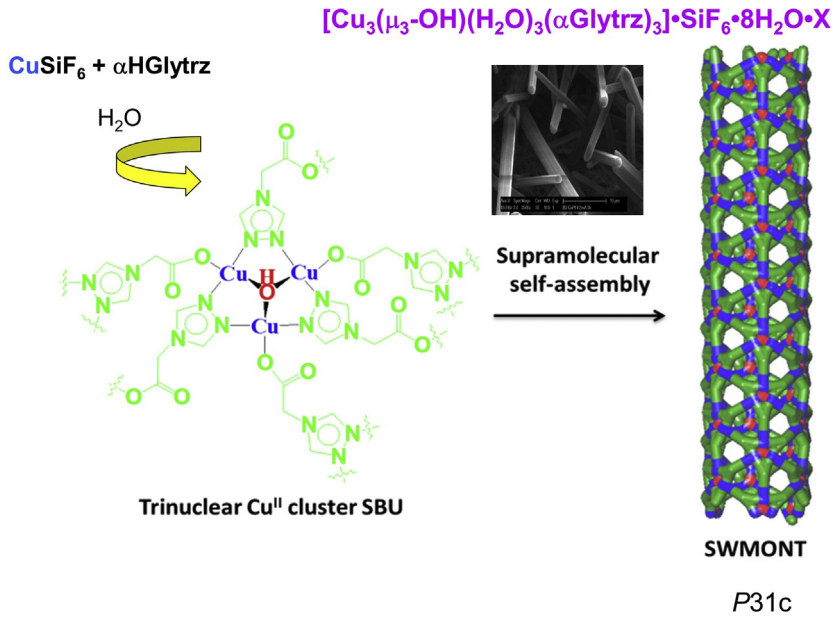

Fig. 1 Synthesis of **9**: a SWMONT obtained from 4H-1,2,4-triazol-4-yl-acetic acid (***αHGlytrz***).[30]

structure are preserved by powder X-ray diffraction. (iii) As thin layers by precipitation/deposition using an electrochemical method, to check its potential to be deposited on a large surface, which could be necessary in case this material would be used in a sensing device. This material, in addition to its unprecedented structure, features a pore size as large as zeolites,[32] thus offering potential, e.g., in gas storage.

Apart from gas storage, which is commonly encountered in MOFs, we have extended its storage properties to metals, in particular metallic mercury by applying Mercury intrusion porosimetry (MIP), a technique which is commonly used in the study of hierarchical porous solids, e.g., for catalytic applications.[33] Indeed, **9** was shown to store metallic mercury, after a moderate pressure treatment, contrary to previous examples (Fig. 2).

The need of a metallic mercury sensor is motivated by the ability of this inorganic element to compromise both respiratory and immune systems,[34a] and lead to neurological, heart and renal dysfunction when it comes into contact with a tissue in sufficient concentration,[34b] thus being considered as threat for public health environment. Interestingly, the chemical composition of **9** completely differs from MIL-53 (Cr), the first reported MOF with mercury storing properties,[35] thus opening a new field of investigation based on chemical design. This material could be used for instance as mercury sponge for household area safety issues, e.g., when children play with shining mercury marbles, coming from old thermometers or domestic lamps.[34a]

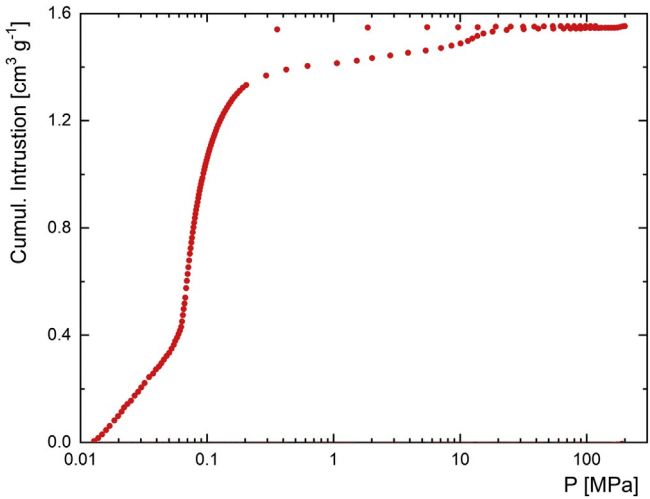

Fig. 2 Metallic mercury intrusion curve in SWMONT **9**.[30]

Apart from metallic mercury capture, Radi *et al*. recently designed a novel hybrid inorganic-organic material (**10**) made of modified silica on which a diamine Schiff base molecule able to capture Hg(II) was immobilized.[36] This hybrid material was prepared firstly by converting a diamine precursor, made of 4-aminophenol and picolinaldehyde in dry ethanol, using acetic acid as catalyst, on an alco-olate salt. This salt was subsequently reacted with a 3-glycidoxypropyltrimethoxysilan
e silylant agent, previously anchored on a silica surface in a heterogeneous manner to yield the target hybrid material (Fig. 3).

This material displayed good thermal stability as well as chemical stability in various acidic and buffer solutions (pH = 1–7). In addition to its porous properties, it presented a retention as high as 98(1) $mg.g^{-1}$ of Hg(II) after five cycles. More interestingly, regeneration was reproducible without destruction of the hybrid matrix by using 5–10 mL of 6 N HCl/g of support.[36] These characteristics offer new opportunities in water cleaning given the range of hybrid materials which could be prepared based on this technology, with interesting sensing properties not only concerning Hg(II) but also Cd(II), Cu(II), Zn(II), Pb(II) to name but a few.[37] In particular, selective properties of such hybrid materials towards a given metal was demonstrated. For instance, coordination of a metal ion (e.g., Cu(II)) was recently supported by a single X-ray diffraction study of a model Cu(II) dinuclear complex.[37b] Such hybrid materials have recently been applied to the cleaning of real water samples originating from two oriental Moroccan rivers: the *Ghiss*, who is known to drop into the *Al Hoceima Gulf*, and the *Touissit-bou-bekker* who is located near *Oujda*, with nearby mining activities recognized to bring enough polluting metals suitable for our investigations.

Pursuing our efforts to investigate the topology and emerging properties of new CPs with azole based ligands, Adarsh *et al*. could grow pale-green block shaped X-ray quality single crystals in reasonable yield (53%) of $[Cu(btzx)_2(MeOH)_2](NO_3)_2$ (**11**) by mixing, in methanol, $Cu(NO_3)_2 \cdot 3H_2O$ and ***btzx*** (Scheme 1) in a 1:2 and even in a 1:3 metal: ligand ratio.[38] The crystal structure of **11** reveals a coordination environment made of two ***btzx*** ligands and two MeOH solvent molecules with Cu-O = 2.2535(14) Å. The designed CuN_4O_2 units laid in a slightly distorted square bipyramidal geometry, with Cu-*N* = 2.0398(16) Å and Cu-*N* = 2.0659(17) Å. Such units are linked to form a 1D looped chain, crystallizing in the triclinic $P\overline{1}$ space group (Fig. 4). The intra metallic Cu⋯Cu distance is 10.238 Å. The polymeric chains recognize the nitrato counter anion via O-H⋯O

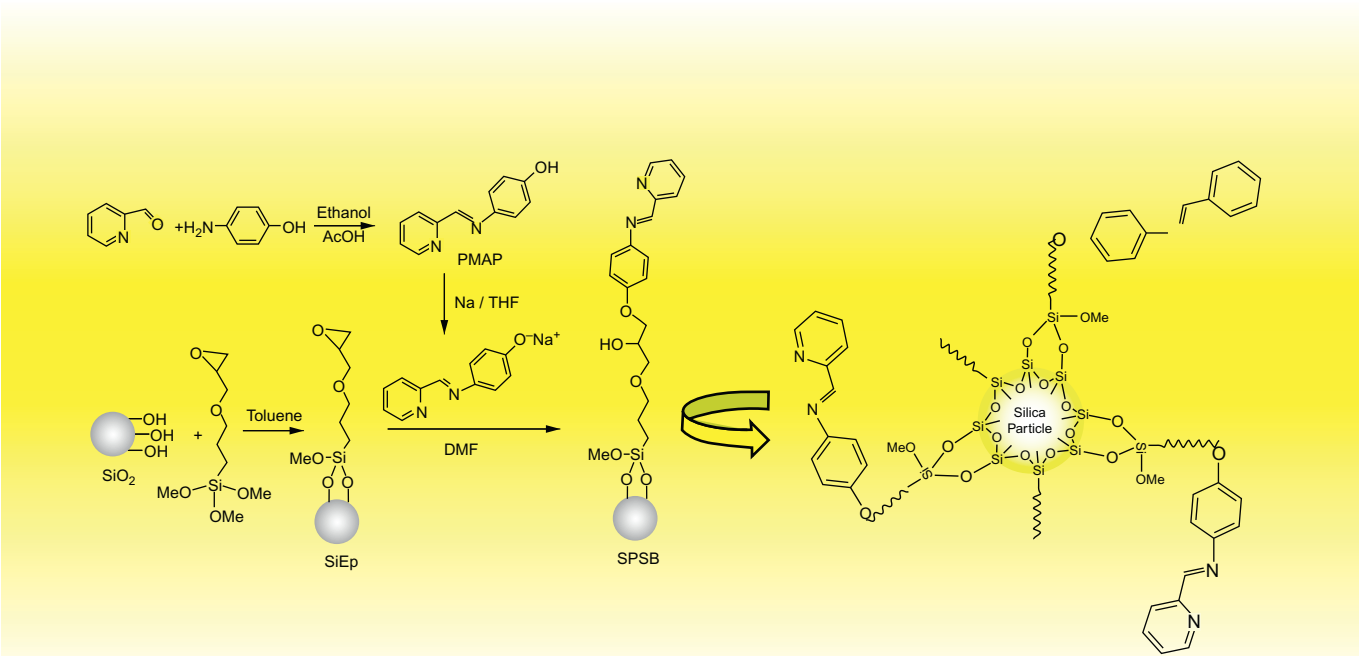

Fig. 3 Synthesis of **10**, a hybrid inorganic-organic silica material able to capture Hg(II).[36]

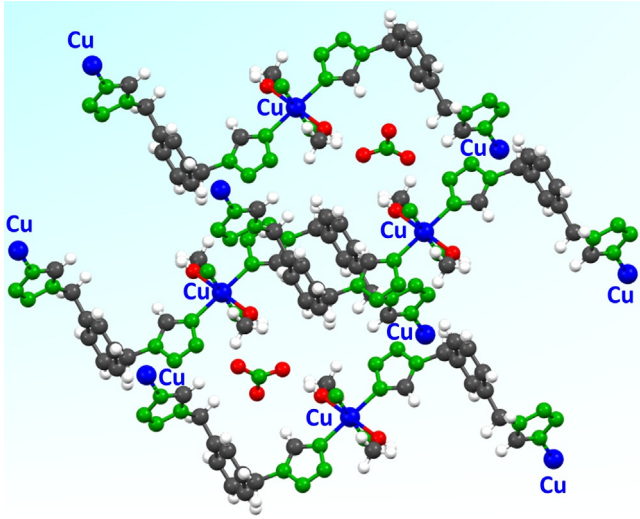

Fig. 4 View of the crystal structure of the 1D looped chain in **11** built from 1,4-bis(-tetrazol-1-ylmethyl)benzene (***btzx***).[38]

hydrogen bonding involving the metal bound methanol molecule [O···O = 2.696(5) Å; ∠O–H···O = 172.52°]. Such chains are packed on top of each other in a slightly off-set fashion sustained by various intermolecular interactions. Worthwhile to note is that the ***btzx*** ligand was previously used in iron(II) coordination chemistry to produce 1D chains.[39] These chains on cooling, displayed gradual SCO profiles due to the flexible and long ***btzx*** spacer between the active spin species, which inefficiently propagate elastic interactions associated with the spin state change. Nevertheless, these materials were found suitable to investigate the influence of gas storage on their SCO properties, in particular with $CO_{2(g)}$.[13]

With the idea of investigating the influence of the chair/boat conformation of cyclohexane on Cu(II) coordination chemistry, we have recently synthesized $[Cu(btrcy)_2(H_2O)_2](ClO_4)_2 \cdot \mathbf{G}$ (***btrcy*** = bis(1,2,4-triazole)-*trans*-cyclohexane; G = ***btrcy*** or 0), which is a 2D network presenting host-guest properties.[38a] Reaction of ***btrcy*** (Scheme 3) with $Cu(ClO_4)_2 \cdot 6H_2O$ in water in a 1:2 ratio afforded a blue precipitate of $[Cu(btrcy)_2(H_2O)_2](ClO_4)_2$ (**12**) which is a 2D network without any guest molecules inclusion. Extension to a 3D network was attempted by reacting $Cu(ClO_4)_2 \cdot 6H_2O$ with a third equivalent of ***btrcy*** in water, which also led to a blue precipitate. Recrystallization from a water/acetone medium provided shining blue colored single crystals after 1 week of slow

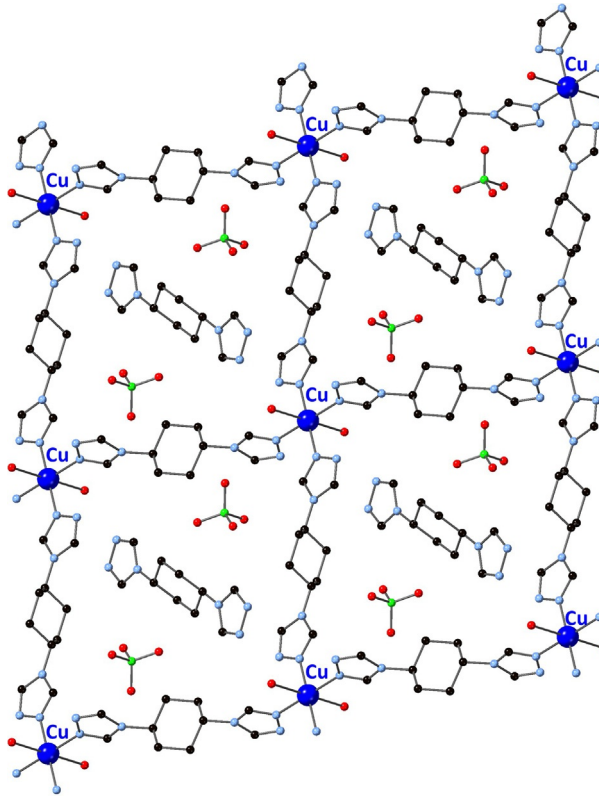

Fig. 5 Projection along the *a* axis of the 2D network **13** incorporating bis(1,2,4-triazole)-*trans*-cyclohexane (***btrcy***) molecules into its voids.[38a]

evaporation at room temperature, contrary to the previous experiment. The single-crystal X-ray diffraction data analysis revealed, however, a 2D-square grid crystallizing into the centrosymmetric triclinic space group $P\overline{1}$. The CP consists of ***btrcy*** connectors around Cu(II) modules coordinated to two water molecules and four ligands leading to CuN_4O_2 chromophores (Fig. 5). Such a Cu(II) coordination environment adopts a square bipyramid geometry, defined by only two Cu—N bond lengths (Cu–N4 = 2.014(2) Å and Cu–N1 = 2.035(2) Å) and one Cu—O bond length (Cu–O1 = 2.431(3) Å). The Cu(II) atoms are bridged by the ligands creating a polymeric 2D structure (Fig. 5). As a result, the shortest Cu ⋯ Cu distances do not bring into play copper atoms from the same layer. Channels are formed which can be considered as squared cavities with a surface of ca. 195 $Å^2$ and a volume equal to the volume of the crystallographic cell (1022 $Å^3$).

Coordination of Cu(II) to water molecules thus prevents the polymerization in the third dimension. Nevertheless, incorporation of three ***btrcy*** molecules was successful, but with an unexpected distribution compared to the target 3D $[Cu(btrcy)_3](ClO_4)_2$ network. Indeed, the formula of our new network is $[Cu(btrcy)_2(H_2O)_2](ClO_4)_2 \cdot$btrcy (**13**) with a ***btrcy*** molecule no more acting as a ligand, but as a guest molecule trapped in the crystal lattice cavities. Indeed, one ***btrcy*** molecule and two perchlorate anions were encapsulated in these cavities (Fig. 5) supported by various H-bonding. The layers are linked to the guest molecules by H-bonding between the water molecules and the nitrogen atoms of the ligand and between the ligands and the perchlorate anions. The perchlorate anions are also involved in H-bonding with the ligand molecules with the same cavity. No relatively short distances are created between neighboring cavity contents. Therefore, the 2D-square grid architecture of **13** is further stabilized by ***btrcy*** molecules trapped as non-coordinated guest molecules in the crystal lattice, through hydrogen bonds involving the coordinated water molecules. Thus, this network is able to host large guest neutral molecules into its voids, a discovery which opens exciting perspectives for sensing guest molecular species which could be hosted into this network.

3. Spin crossover materials

Apart from bis-1,2,4-triazole chemistry, our group has recently focused on a reborn material made of Fe(II) nodes and the spider like tris-tetrazole ligand, ***N(entz)$_3$*** = tris[(tetrazole-1-yl)ethane]amine (Scheme 4).[40]

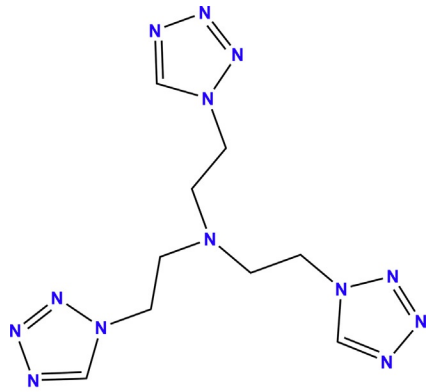

N(entz)$_3$

Scheme 4 Molecular structures of ***N(entz)$_3$*** and ***trz-tzH***.

This 2D material, $[Fe\{N(entz)_3\}_2](BF_4)_2$ (**14**) whose topology was first evidenced by Bronisz *et al.* during his PhD work,[41] represents the first spin transition grid built from a 1R-tetrazole ligand. It displays on cooling a sharp, hysteretic and complete SCO behavior with $T_C^{\downarrow} = 167$ K and $T_C^{\uparrow} = 176$ K. Reaction of ***N(entz)₃*** in acetonitrile with $[Fe(H_2O)_6](ClO_4)_2$ in 2:1 ratio lead to a clear solution, which after 1 week evaporation under darkness provided block shaped colorless crystals.[42] Single crystal X-ray diffraction analysis revealed 2D-corrugated sheets along the *b* axis, for $[Fe\{N(entz)_3\}_2](ClO_4)_2$ (**15**) crystallizing in the P-1 space group (Fig. 6). At 250 K, the Fe—N bong lengths were found to be 2.175–2.204 Å, which are typical for Fe(II) ions in the HS state. On cooling to 110 K, Fe-*N* = 1.992–1.998 Å, which is characteristic for Fe(II) LS ions.

Confirmation of a HS to LS transition was made by Mössbauer spectroscopy that revealed at room temperature, a quadrupole doublet with isomer

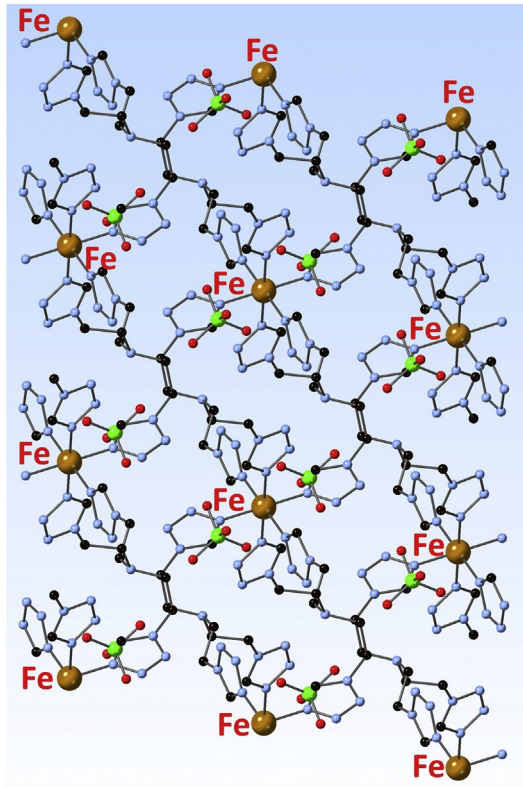

Fig. 6 View of the crystal structure of the 2D Fe(II) tris[(tetrazole-1-yl)ethane]amine (***N(entz)₃***) network (**15**) in the LS state, recorded at 110 K.[42]

shift $\delta^{HS} = 1.07(1)$ mm/s and quadrupole splitting $\Delta E_Q^{HS} = 1.46(1)$ mm/s typical of Fe(II) HS ions. Reduction of both isomer shifts and quadrupole splitting was observed at 78 K with $\delta^{LS} = 0.59(1)$ mm/s and $\Delta E_Q^{LS} = 0.21(1)$ mm/s, which are typical parameters for Fe(II) LS ions. Integration of the surface area of the Mössbauer spectra, assuming equal Debye Waller factors for HS and LS states, provided the temperature dependence evolution of the HS molar fraction. A steep, complete and hysteretic spin transition, shifted downwards compared to the BF_4^- derivative, with $T_C^{\downarrow} = 149$ K and $T_C^{\uparrow} = 170$ K, was observed (Fig. 7). This material displays in addition reversible thermochromism from white (room temperature) to violet (at liquid nitrogen temperature),[43] a feature which was preserved for the thin film obtained by drop casting an aqueous colloidal dispersion of flakes of this material into a poly(vinyl alcohol) matrix.[42]

Indeed, such appealing SCO properties combined to the 2D character of this material made it a candidate for a delamination study in view to ease its future implementation into spintronic devices, a field which has been recently reviewed.[44] Large size crystals were selected by Suarez-Garcia *et al.* and subsequently delaminated using an ultrasonic treatment followed by liquid-phase exfoliation using an orbital shaker. Centrifugation afforded stable colloidal suspensions of 2D flakes.[42]

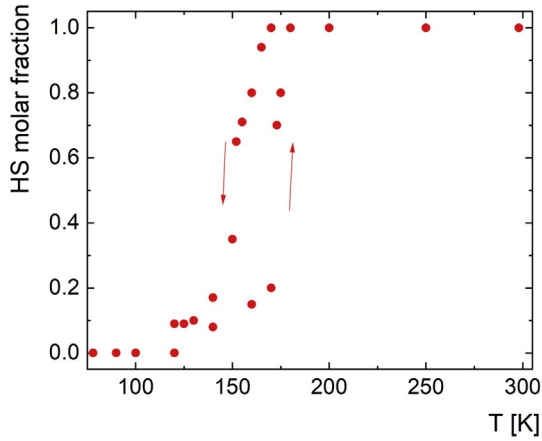

Fig. 7 Bistability domain as seen by the temperature dependence of the HS molar fraction for **15**.[43]

4. Crystal network design

Combing back to CPs design, the tetrafluoroborate anion has been used as template to precipitate/crystallize a number of cationic CPs and MOFs. It is known to be non-coordinating, with many reported examples, e.g., in Zn(II) complexes.[45–48] In addition, it is readily available in a number of metal salts and can be prepared easily from HBF_4 acid. It is preferred, along with the PF_6^- anion, to the perchlorate anion which is known to be potentially explosive.[49] The number of molecular complexes including coordinated BF_4 is rather weak due to the low coordination strength of metal-fluoro bonds, contrary to metal fluorides, e.g., $ZnF_2{\bullet}2H_2O$.[50] In particular, relatively few examples of Zn(II) complexes with coordinated BF_4^- anions have been reported. The list includes mononuclear complexes with monodentate coordination,[51–54] or μ_2 coordination,[55] as well as dinuclear complexes with mono coordination,[56–60] and μ_2 coordination,[61] a pentamer,[62] as well as an octamer.[63] This feature is interesting to block the propagation of a CP in the three space dimensions. Along this line, we have recently reported the first example of Zn(II) CP with a coordinated BF_4^- anion, which crystallized in a 1D coordination polymer.[64] Indeed, the reaction of $Zn(BF_4)_2 \cdot 6H_2O$ with acyclic cryptate-bis(1*H*-1,2,4-triazole) (***acbtr***) ligand (Scheme 3) in a 1:3 ratio in methanol yielded the 1D CP $Zn(acbtr)_2(BF_4)_2$, (**16**) which was crystallized in the monoclinic space group, *C*2/*m*.

The Zn(II) metal center sits in a slightly distorted octahedral geometry while the Zn(II) equatorial positions are occupied by the N atoms of the ligand. For **16**, Zn-*N* = 2.115(5) Å, which is longer than the bond lengths found in the dinuclear complex $[Zn_2(ptpp)_2]0.5EtOH$ (**17**) (***ptpp*** = (*E*)-2-({2-[3-(pyridin-2-yl)-1H-1,2,4-triazol-5-yl]phenylimino}methyl)phenol), or its polymorph, with Zn-*N* = 2.094 Å and 2.052 Å, respectively.[65,66] The Zn—N bond length is however shorter compared to the neutral trinuclear 1,2,4-triazole complex $[Zn_3(mttba)_6(H_2O)_6]$ (**18**) (***mttba*** = 4-(methylthio)-2-(4H-1,2,4-triazol-4-yl)butanoic acid, Scheme 2) with Zn-*N* = 2.159(4) Å and 2.145(4) Å.[67] The apical positions of Zn(II) are occupied with F atoms belonging to BF_4^- anions, with Zn-F = 2.178(7) Å. This bond length is in rather good agreement with the one of a dinuclear Zn(II) complex with Zn-F = 2.187 Å.[56] The ligand exhibits energetically less favorable *syn-syn* conformation around the aliphatic chain and keeps the 1,2,4-triazole rings *syn* to each other. Moreover the terminal 1,2,4-triazole rings coordinated to Zn(II) were oriented in a *syn* fashion resulting in an "W" shaped

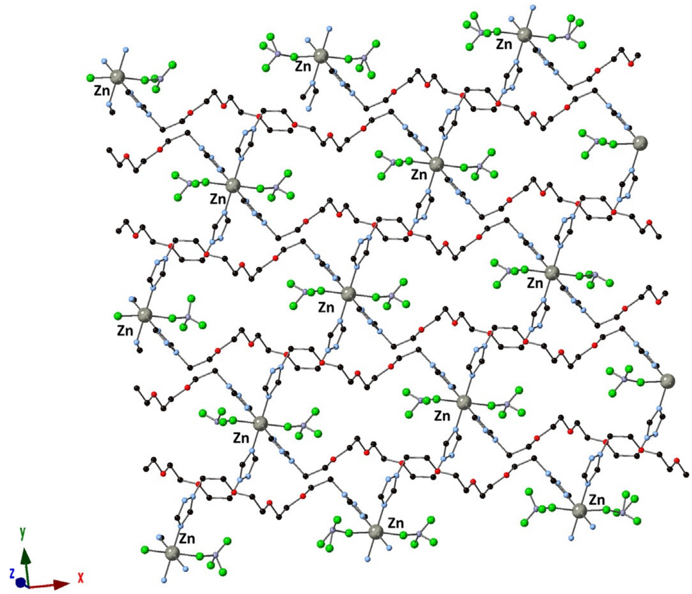

Fig. 8 Projection of the crystal structure of **16** showing 1D chains with the long acyclic cryptate-bis(1*H*-1,2,4-triazole) (***acbtr***) ligand.[64]

ligating topology. The conformational dependent "W" shaped ligating topology of the ligand, metal: ligand ratio (1:1), and coordination mode of the counter anion, leads to the formation of a 1D looped chain coordination polymer. C—H···F hydrogen bonding interaction was found in **16** involving the metal bound BF_4^- and C—H of the 1,2,4-triazole ring, which helped to stabilize the 1D looped CP chains (Fig. 8).

Reaction of ***acbtr*** with $Cu(NO_3)_2 \cdot 3H_2O$ in methanol led to the isostructural $Cu(acbtr)_2(NO_3)_2$ (**19**). The metal bound nitrate anion is connected to the C—H of a 1,2,4-triazole ring through a C—H···O interaction, which allows to consider this 1D looped chain as a 2D supramolecular polymer. Compound **19** represents a rare example of nitrato anion coordination in Cu(II) bis-triazole CPs. Few examples have been discovered including a 2D network, $[Cu(btr)_2(NO_3)_2]\cdot H_2O$ (**20**) and a 1D chain $[Cu_2(OH)(btrad)_2](NO_3)_3\cdot 4H_2O$ (**21**) (***btrad*** = 1,3-bis(1,2,4-triazol-4-yl)-adamantane, Scheme 3) where nitrato anions are weakly coordinated with Cu-O = 2.747 Å,[68] and 2.768 Å,[69] respectively, contrary to **19** which shows a shorter distance with Cu-O = 2.447 Å. The situation differs for the 1D chain $[Cu(btrb)NO_3](NO_3)\cdot 2H_2O$ (**22**) with ***btrb*** = 1,3-di-(1,2,4-triazole-4-yl)

benzene, Scheme 3), where the nitrato anions μ_2-bridge the Cu(II) ions, with expected shorter Cu-O(NO_2) bond lengths of 2.3 Å.[70]

Sacrificial thermal treatment of molecular precursors is considered as a low energy consuming as well as straightforward method to produce metal oxides in powdered form, provided the molecular precursors are available in a decent amount, e.g., starting from polyaminocarboxylate metal complexes.[71] This method was only recently extended to CP and MOFs, e.g., to produce the β phase of CdO from the chain $[Cd_2(Glytrz)_2Cl_2]$ (**23**).[28a] Thermal treatment up to 537 °C of **16** and **19** afforded ZnO and CuO oxides, respectively.

Reaction of d^{10} transition metals (Zn(II), Cd(II) or Hg(II)) with flexible bent bis-1,2,4-triazole based ligands led to a set of CPs and mononuclear complexes of diverse topologies, which all display solid state blue luminescence at room temperature. Reaction of Zn(II) ions with ***btpm*** = bis (4-(1,2,4-triazol-4-yl)phenyl)methane (Scheme 3), a symmetric molecule prone to coordinate up to four metal centers to lead to multidimensional CPs, yielded a 1D chain $[ZnCl_2(btpm)]$ (**24**) (*P*–1) and a 2D square-grid $[Zn(btpm)_2(H_2O)](BF_4)_2{\cdot}2(btpm){\cdot}8H_2O$ (**25**) ($P2_12_12$). It is striking that such a diverse topology can be obtained while only modifying the reacting counter anion. Indeed, recrystallization from water of the precipitate obtained by the self-assembly of ***btpm*** with $ZnCl_2$ afforded the linear 1D CP (**24**) by repetition of $ZnCl_2$(btpm) units, with a bidentate bridging ***btpm*** spacer coordinating two tetrahedral Zn nodes, spaced out by 15.18(2) Å. Substitution of chloride by a weakly coordinating BF_4 anion resulted in the 2D CP (**25**). In **25**, ***btpm*** coordinates as in **24**, but four ligands are arranged around every Zn(II) cation, and a coordinated water molecule completes the coordination sphere. Given that a crystallographic twofold symmetry axis coincides with the $Zn-OH_2$ axis, the complex could be described as a distorted square pyramid, where the coordinated water molecule occupies the axial position. The distortion parameter τ_4 of 0.69, however, fits better with a trigonal-pyramidal geometry.[72] Working under hydrothermal conditions with $M(NO_3)_2$ (M = Zn, Cd) instead, led to the CP $[M_2(btpm)_3(H_2O)_4](NO_3)_4{\cdot}nH_2O$ (**26**) (M = Zn, $n = 1$ or M = Cd, $n = 3.5$),[73] whose crystal structure shows interpenetrating sheets with octahedral Zn nodes, confirming the influence of the synthetic conditions on the overall topology.

Reaction of a strongly coordinating anion, such as $CdCl_2$, under solvothermal conditions, resulted instead in a 1D chain, $[Cd_3Cl_6(btpm)_2]{\cdot}8H_2O$ (**27**) (*P*–1).[74] This compound only shows the μ_4-tetradentate coordination mode, and a bridging Cl anion. **27** forms a polymeric 1D chain

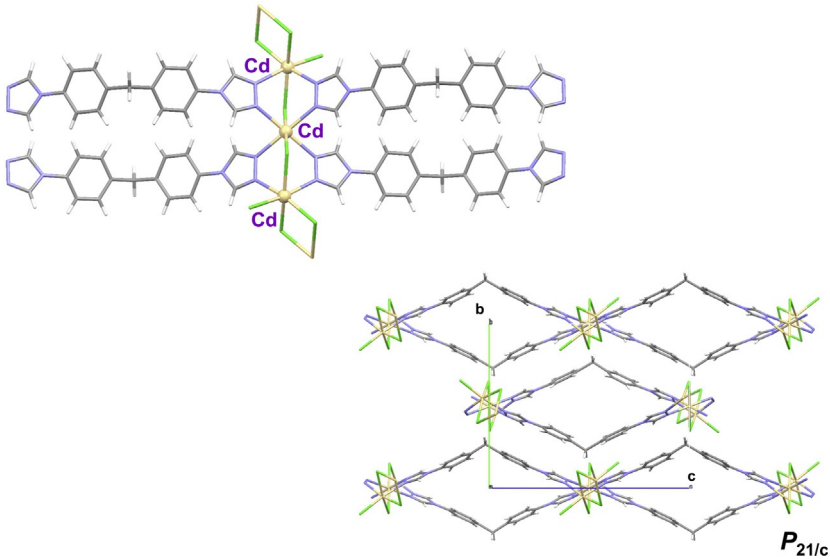

Fig. 9 View of the 2D bi waved polymer **27** built from bis(4-(1,2,4-triazol-4-yl)phenyl) methane (***btmp***).[74]

by repetition of linear tri-nuclear Cd units; the central Cd(II) ion is located on an inversion center and on either side it is coordinated by two bridging 1,2,4-triazole moieties and a bridging Cl atom, adopting a distorted octahedron. The terminal Cd(II) ions are also found in octahedral environments which are completed by three Cl atoms; two of these are bridging with a neighboring tri-nuclear unit, and one is a terminal Cl atom (Fig. 9).

Reaction with the newly designed ligand, ***ppt*** = 4-phenoxyphenyl-1,2,4-triazole (Scheme 2), afforded mononuclear complexes $[MCl_2(ppt)_2]$ (M = Zn, Hg) which crystallize in the *I2* (**28**) and *C2* (**29**) space groups, respectively. These were obtained following two crystallization methods, hydrothermal and slow diffusion, respectively. In each case, the metal ion is bound to one nitrogen atom belonging to two ppt ligands, as well as two chloride anions. A bivalent cationic 1D CP was, however, observed with Cd(II). $[Cd_2Cl_2(ppt)_4]CdCl_4 \cdot 4DMF$ (**30**) crystallizes in the *P-1* space group, with the inclusion of a non-coordinated $CdCl_4^{2-}$ anion which formed *in situ* (Fig. 10).

The use of the new bridging ligand, ***tpca*** = *N*-(1,2,4-triazol-4-yl)pyridine-3-carboxamide (Scheme 2) afforded two 1D chains of formula $[MCl_2(tpca)]$ (M = Zn (**31**) and Hg (**32**)) ($P2_1/c$) along with the 2D net, $[Cd(tpca)_2(H_2O)_2] \cdot 2H_2O$ (*C*2/c) (**33**).[74]

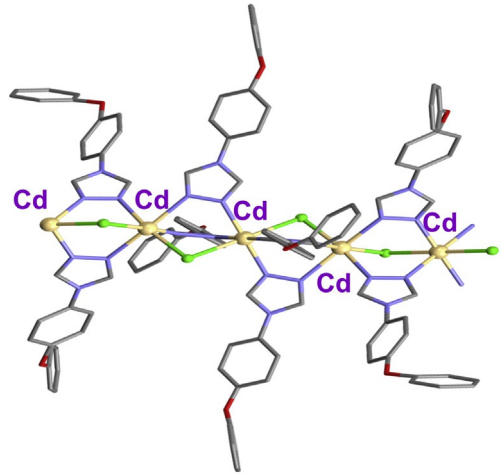

Fig. 10 View of the 1D chain **30** built from 4-phenoxyphenyl-1,2,4-triazole (***ppt***). $CdCl_4^{2-}$ anions were omitted for clarity.[74]

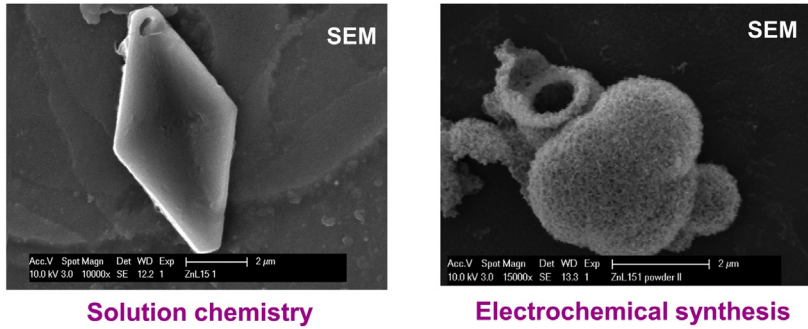

Fig. 11 Synthesis of single crystals (left) by solution chemistry or balls of coccolith morphology (right) by electrochemical synthesis of **25**.[74]

Electrochemical synthesis of such materials was demonstrated, e.g., on **25**, which constitutes a rare example of the successful application of this preparation method to CPs, a method which has been seldom applied to synthesize MOFs.[35,75] Hollow spherical clusters with micrometric dimensions were identified by scanning electron microscopy. Magnification shows hollow structures of ~1 μm diameter with potential porous properties (Fig. 11).[74] Interestingly, such spherical structuration was observed earlier on a bulk sample of $[Zn(trzg)_2Cl_2]Cl_2{\cdot}H_2O$ (**34**)

(***trzg*** = *N*-4*H*-1,2,4-triazol-4-yl-guanidine hydrochloride, Scheme 2), with porous balls of coccolith morphology with surface decorated sickle-shaped particles of ~100 nm thickness.[28a]

Pursuing our efforts in CPs synthesis, we have applied our revised trans-amination method,[26] to introduce a dissymmetric azole molecule, ***trz-tzH*** (5-(4H-1,2,4-triazol-yl)-2H-tetrazole, Scheme 4). This molecule with a high nitrogen content (~72%) can be compared to 5,5′-bistetrazole (***H_2btz***) and 1,5′-bistetrazole (***Hbtz)*** (Scheme 1).[76]

Such molecules can be considered as high energetic materials for low smoke pyrotechnics due to a combination of a fuel and a colorant in a single compound.[77] The synthesis of ***trz-tzH*** was done in one step from *N*,*N*′-dimethyl-formamide azine dihydrochloric acid in refluxing toluene overnight with 5-amino-tetrazole to lead to the target molecule in 70% yield.[26] Starting from *N*,*N*′-dimethyl-formamide azine in refluxing benzene afforded the target molecule in higher yield (79%).[78] Reaction of ***trz-tzH*** in water with M(OH) (M = Li, Na, K) yielded two alkali CPs. For instance, the crystal structure of [Li(trz-tz)H_2O] (**35**) reveals 1D chains of tetrahedrally coordinated Li^+ ion with two nitrogen atoms of the 1,2,4-triazole fragments belonging to two ***trz-tz*** anions and two water oxygen atoms (Fig. 12). The triazole fragments of the anionic ligands each coordinate two lithium cations in a bridging μ^2-*N*3,*N*4-coordination mode with the Li–N–N–Li torsion angle being 18.7(7)°. The bicyclic ligands are essentially planar, the dihedral

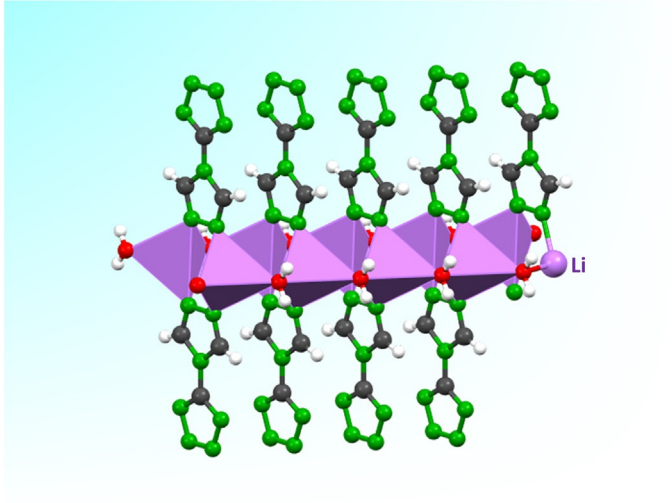

Fig. 12 View of the 1D chain **35** built from anionic ***trz-tz*** ligands.[79]

angle between triazole and tetrazole fragments being only 1.2(3)°. All ***trz-tz*** ligands are therefore coordinated almost orthogonally to the 1D chain axis (Fig. 12). The water molecules link two neighboring cations with a bridging μ^2-*O*-coordination mode. The Li—Li distances along and across the 1D chain are 3.434(15) and 3.535(16) Å, respectively, while the Li–O–Li and O–Li–O angles are equal to 117.9(6)°. Every 1D polymeric chain is connected to four neighboring chains through O–H⋯N hydrogen bonds, via a water molecule and *N*2 and *N*4 nitrogen atoms of the tetrazole cycles, thus forming a supramolecular network.[79]

Reaction of ***trz-tzH*** in water with $M(OH)_2$ (M = Mg, Ca) affords alkaline earth salts and a CP with M = Ba.[79] For the salt, $[Mg(H_2O)_6](trz\text{-}tz)_2$ (**36**), the magnesium ion is surrounded by six water molecules octahedrally coordinated while in $[Ca(H_2O)_8](trz\text{-}tz)_2$ (**37**) a square antiprism is formed with eight water molecules. In both structures, layers formed by the corresponding cationic parts $[Mg(H_2O)_6]^{2+}$ or $[Ca(H_2O)_8]^{2+}$, are separated by layers of anions ***trz-tz***. In **36**, the anions are, however, cross-packed whereas in $[Ca(H_2O)_8](trz\text{-}tz)_2$ they are packed parallel to each other (Fig. 13). Both structures contain an extensive hydrogen bonds network, which is also supported by the anions ***trz-tz***. The latter molecules are also stabilized by a number of π⋯π interactions.

The crystal structure of the CP $[Ba_2(trz\text{-}tz)_4(H_2O)_9]$ (**38**) comprises 1D polymeric chains, built from two different barium-containing building units. Both metal centers are nine-coordinated with the formation of mono-capped square anti-prismatic coordination polyhedra. The Ba(1) cation is coordinated by four nitrogen atoms originating from two *N*2-coordinated tetrazole and two μ^2-*N*1,*N*2-coordinated tri-azole rings,

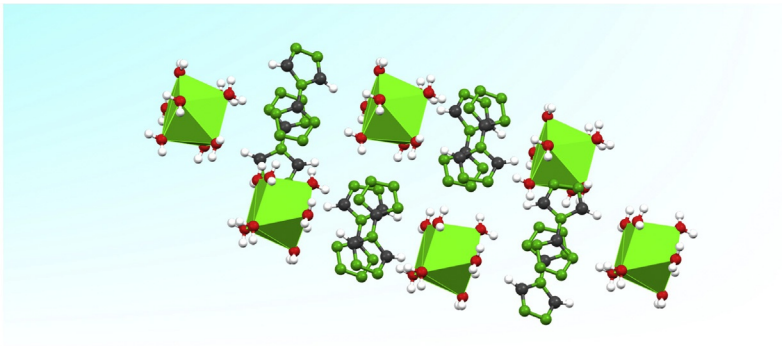

Fig. 13 View of mononuclear calcium units with ***trz-tz*** counteranions in **37**.[79]

corresponding to four different ***trz-tz*** anions. Two of these anionic ligands serve as bridging ligands between Ba(II) cations, connecting them through the triazole *N*1,*N*2-nitrogen atoms. The coordination environment of the Ba(1) cation is completed by two terminally coordinated and three μ^2-*O*-coordinated water molecules. The latter water molecules also participate in the coordination with Ba(2), which coordination environment is further completed by four terminal water molecules. Neighboring 1D chains are interpenetrated with each other and stabilized by a network of O–H⋯N hydrogen bonds as well as a number of $\pi\cdots\pi$ interactions, formed by the ***trz-tz*** heterocycles.

5. Sensing toxic industrial chemicals

There is currently a huge interest for "chemo-sensors" based on colorimetric sensor array (CSA) technology for the sensitive and selective detection of gas- and vapor-phase analytes. Such sensors are actively developed to reply to current needs of our society in terms of detection, particularly of toxic threats in food, air, surfaces, for medical diagnostics, and environmental monitoring. These sensor materials always incorporate a targeted set of chemically responsive colorants. Currently, coordination complexes are developed for colorimetric detection of metal-binding species, especially, toxic small molecules such as amines, covalent hydrides and alcohols. It mainly benefits from two contributions of metalo-colorants: (a) in well documented examples, analytes can directly coordinate to the metal center, causing significant changes to the d − d absorptions, and thus to the sensor color; (b) metal center can respond to redox reactions, thus provoking a sensor color change. Optical detection, in particular visible one, is the most demanded since it does not require sophisticated detection systems. Classic approaches consist of using irreversible color change due to metal or ligand oxidation. In this respect, iron sensors offer a large panel of possibilities due to their various spin and oxidation states. For instance, Fe(II) salts can oxidize in air from colorless to yellow/brown and can be used straightforwardly. More challenging are detectors which can offer different color sets depending on the probed analyte, as well as unlimited regeneration.

Reaction of $[Fe(H_2O)_6]A_2$ ($A = BF_4^-$, ClO_4^-) in water with ***trz-tzH*** at neutral pH afforded an air stable microcrystalline complex. Single crystal X-ray diffraction revealed a mononuclear Fe(II) neutral complex, $[Fe(trz\text{-}tz)_2(H_2O)_4]\cdot 4H_2O$ (**39**) which crystallizes in the P-1 space group (Fig. 14).[78]

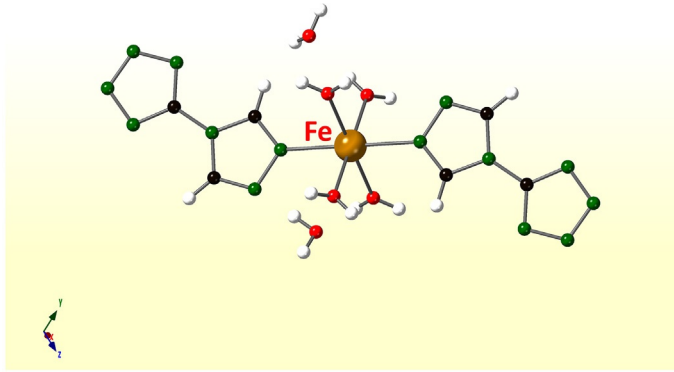

Fig. 14 View of the mononuclear iron(II) ***trz-tz*** complex **39**.[78]

In this molecule, two ***trz-tz*** ligands are bound through the N1 of the 1,2,4-triazole units to Fe(II), while four water molecules complete the octahedral coordination sphere. No counter anions are observed due to tetrazole deprotonation upon complexation, which balances the charge of the metal cation. The presence of coordinated water molecules in the coordination sphere sets a weak ligand field around the iron, which prevents any possibility of thermally induced spin switching. At room temperature, a large quadrupole doublet typical of the HS state, with $\delta = 1.17(2)$ mm/s and $\Delta E_Q = 3.18$ mm/s, is observed by ^{57}Fe Mössbauer spectroscopy. The HS state is also confirmed by X-ray diffraction with Fe-$N = 2.182(5)$ Å and Fe-O = 2.094(4) Å and 2.182(5) Å. Such material was screened for colorimetric sensing abilities for a wide spectrum of vapor-phase analytes (MeOH, EtOH) including toxic gases (HCl, HBr, hydrazine monohydrate, ammonia). Although pellet **39** possesses a single sensing unit without any other cross-reactive elements, it can capture information about analyte molecules in a distributed fashion that is encoded sufficiently to allow discrimination from other closely related chemical structures. In particular, the pink color detection (e.g., obtained with $MeOH_{(g)}$) was systematically associated to the emergence of $Fe^{II}N_6$ LS ions as shown by diffuse reflectance spectroscopy and ^{57}Fe Mössbauer spectroscopy.[78] Clear color differentiation among four different toxic industrial chemicals (TICs) and alcohols was demonstrated. Different TICs and alcohols were readily identified using a standard chemometric approach (hierarchical clustering analysis), with no misclassifications over 18 trials. ^{57}Fe Mössbauer spectroscopy was applied to investigate the driving spin state change of the analytes in this Fe-azole sensor material.[80] In particular, comparison was made before and after analyte

sensing. When the native hydrate sensor pellet **39** was in contact with $MeOH_{(l)}$, it turned instantly from white to pale pink. When the pellet was subjected to $MeOH_{(g)}$, it was transformed to the same pink color within 5 min, but took hours to be converted into dark pink until the material was saturated with $MeOH_{(g)}$. Remarkably, when MeOH was removed under vacuum at room temperature, the material did not return to its initial color and stayed pink. This MeOH removal was not associated with any spin state and iron coordination sphere modification as show by ^{57}Fe Mössbauer spectra recorded before and after pumping. Interestingly, this material turned back to white when exposed to water vapor or washed with water, with full iron site regeneration, as also shown by ^{57}Fe Mössbauer spectroscopy. **39** thus detects MeOH with a memory effect by visual, optical and magnetic feedback.[80] This material behaves much different from classic alcohols sensors, where control over the memory effect is unlikely because of the fake of analyte departure from the material. Indeed, after experiencing a color change due to guest molecule detection, the color is lost upon guest release. This situation holds for various Fe(II) spin crossover materials reported up to know.[81,82] Sensor **39** keeps, however, the color associated with alcohol detection, even after its full release from the material. Does size play a role for this coordination system regarding alcohol detection? Actually, the selectivity of detection decreases in the order MeOH > EtOH > i-PrOH > with increasing alcohol molecule size, and no color change was observed for higher size alcohol analogues (o-PrOH, BuOH, pentan-1-ol).[78] A weaker vapochromic behavior was indeed noticed when a pellet of **39** was exposed to EtOH vapors. Contrary to $MeOH_{(g)}$, the response time lasted much longer (2 days). Such a color change was only observed as a slight effect on the crystal surface of **39** when exposed to $EtOH_{(g)}$, presumably due to the lower available surface area.[78] Apart from alcohols, acid sensing was also studied, among other toxic chemicals. Although acetic, nitric, sulfuric and perchloric acids were not detected at all by this sensor, clear color changes to yellow and orange were observed for $HCl_{(g)}$ and $HBr_{(g)}$, respectively. Surprisingly no change was observed in the isomer shift, δ, deduced from Mössbauer spectra before and after gas uptake. This indicates that no change was provoked in the iron coordination sphere. Rather a protonation of tetrazole units leading to ***trz-tzH*** along with inclusion of halide anions is suggested. More surprising, is the Mössbauer spectrum after $NH_{3(g)}$ contact which shows the occurrence of iron(II) LS ions, with $\delta = 0.36(3)$ mm/s and $\Delta E_Q = 0.65(5)$ mm/s. Since NH_3 is known to set up a weak ligand field strength according to the spectrochemical series, as for

MeOH or EtOH, a similar mechanism valid for alcohol should also apply. This may imply reversible coordination of neighboring tetrazole ligands, a hypothesis currently under extensive investigation in our laboratory. This innovative approach opens up perspectives for the further development of iron materials as potential optical sensor arrays through colorimetric techniques, given the potential of molecules to be explored.[83]

6. Nanomedicine

Biomedical application of nanoscale materials for diagnosis and therapy is considered as a promising field of research where coordination chemistry could play a driving role. In particular, the design and synthesis of nanoscale CPs (NCPs) has become an intensive field of investigation.[84–87] The tune ability of supramolecular architectures through self-assembly processes of metallic ions with polydentate bridging ligands, has allowed to obtain a large set of nanoparticles with specific target properties, for instance for tumor immunotherapy.[88] Among bis-azole coordination networks, the use of bis-imidazole linkers allowed to produce a considerable amount of CPS and MOFs.[89] Recently, Adarsh *et al.* reviewed CPs built from 1,4-bis (imidazol-1-yl-methyl)benzene (***bimb***, Scheme 5).[90]

Despite the synthetic advances, challenging steps concern the design of surface functionalization of NCPs in order to improve their colloidal stability, biocompatibility and circulation time in blood, which are crucial for any optimized therapy. Within this frame, the group of Ruiz-Molina has made several advances, including the design of fluorescent dyes functionalized onto NPs in order to enable cellular uptake and monitoring. This applies for instance for dual fluorescent NCPs,[91] novel dual T_1/ T_2 NCPs as novel contrast agents for MRI in the treatment of brain tumor,[92] as well as Pt(IV) based NPCS,[93] to name but a few.

Surface decoration of NPs offer many advantages including the fine-tuning of solubility, biocompatibility and other properties such as, e.g., anti-oxidant and anti-bacterial properties. In particular, pyrazoles and benzimidazoles are present in many pharmaceuticals with a wide range of biological activities,[94–96] including potential activity against the proliferation of human tumor cells.[97] Benzimidazole complexes have been explored for their biological activity,[98] some having revealed relatively high antibacterial and antifungal properties.[99] For instance, zinc complexes, have been used, in addition to their antimicrobial activity, as anti-cancer agents for *in vitro* and *in vivo* studies, and have been shown to play an important role in the

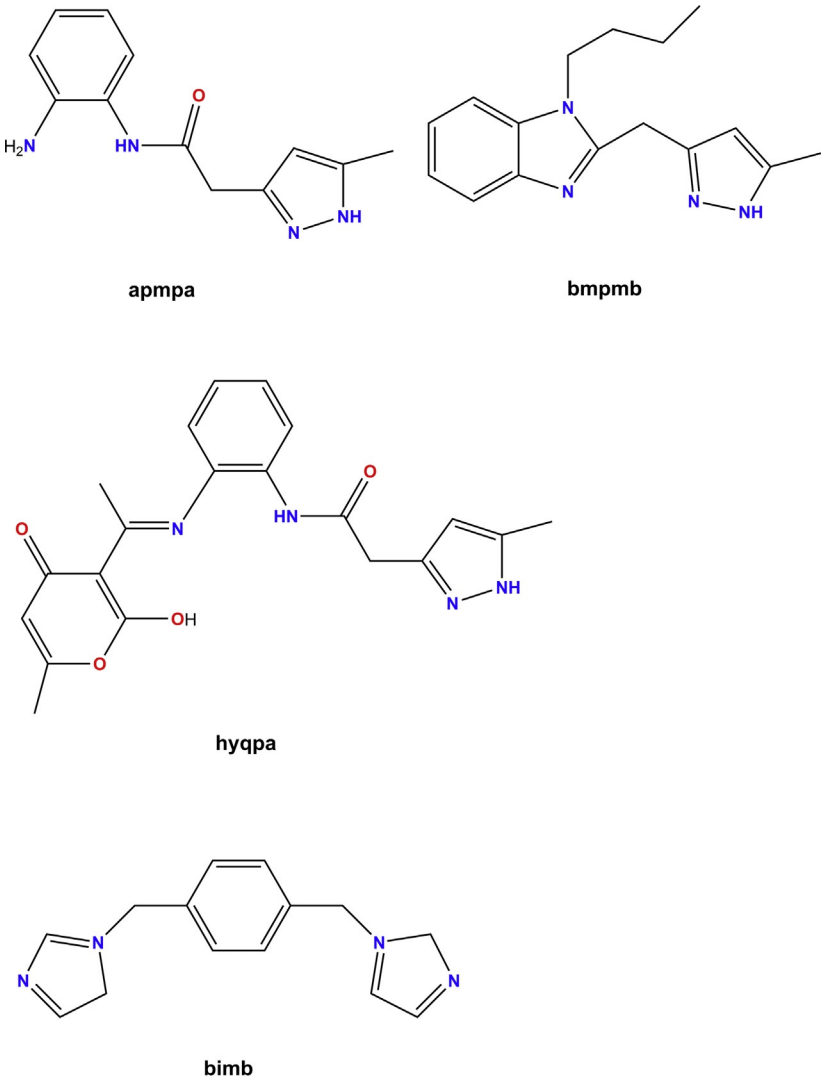

Scheme 5 Molecular structures of selected pyrazole and imidazole molecules.

chemotherapeutic process.[100] Other metal complexes have shown a significant cytotoxic activity, to name but a few.[101] Pyrazole derivatives are from their side known for their antimicrobial activities,[102] among many other properties. Along this line, Chkirate *et al.*[103] recently synthesized two mononuclear complexes $[Co(apmpa)_2(EtOH)_2]\cdot Cl_2$ (**40**) and $[Cu(hqpa)]\cdot H_2O$ (**41**), based on pyrazole-acetamide derivatives, namely *N*-(2-aminophenyl)-2-(5-methyl-1H-pyrazol-3-yl) acetamide (***apmpa***) and

(*E*)-*N*-(2-(1-(2-hydroxy-6-methyl-4-oxo-4H-pyran-3-yl)ethylideneamino) phenyl)-2-(5-methyl-1H-pyrazol-3-yl) acetamide (***hqpa***) (Scheme 5).

The crystal structures of **40** and **41** revealed 1D and 2D supramolecular architectures, respectively, via various hydrogen bonding interactions. Furthermore, the antioxidant activity of the ligands and their complexes were determined in vitro in different concentration ranges by 1,1-diphenyl-2-picrylhydrazyl (DPPH) and 2,2′-azino-bis(3-ethylbenzothiazoline-6-sulphonic acid (ABTS) radicals, and ferric reducing antioxidant power (FRAP) test. Significant antioxidant activity were recorded compared to literature references.[103]

Chkirate *et al.* extended their studies to pyrazole-benzimidazole derivatives by preparing three mononuclear coordination complexes of 1-butyl-2-((5-methyl-1H-pyrazol-3-yl)methyl)-1H-benzimidazole (***bmpmb***, Scheme 5) namely two pseudo-polymorphs $[Co(bmpmb)]Cl_2$ (**42**) and $[Co_2(bmpmb)_2]Cl_2{\cdot}H_2O$ (**43**) as well as $[Zn_2(bmpmb)_2]Cl_2$. Single crystals X-ray diffraction revealed that the presence of N—H···Cl and C—H···Cl hydrogen bonding in the crystal structure of $[M(bmpmb)]Cl_2$ (M = Co, Zn) assist the formation of a 2D hydrogen bonded sheet (M = Co) and an orthogonal packed (M = Zn) [2D sheet + a pair of 1D chain], leading to supramolecular structures. A combination of N—H···Cl, C—H···Cl, O—H···Cl, C—H···O interactions results, however, in a 2D corrugated hydrogen bonded sheet with inclusion of water molecules in **43**. Hirshfeld surface analysis confirmed the presence of various hydrogen bonding and π-stacking interactions, stabilizing the crystal structures.[104]

Noticeably, antibacterial activity against the strains of *Escherichia coli*, *Pseudomonas aeruginosa* and *Staphylocoque aureus* bacteria, was revealed for these complexes. In particular, a normalized minimum inhibitory concentration as low as 6.25 μg/mL s was recorded for **43**, even better than the antibiotic chloramphenicol.[104] This result correlates very well with its crystal structure determined by X-ray diffraction, which revealed a lattice included water molecule, which is one of the key factors for crystalline anti-bacterial properties. Indeed, crystalline materials having lattice included water molecules were reported to have more antibacterial activity, due to the hydrophilic attraction of the bacteria cell wall.[105]

7. Conclusions and future developments

In this contribution, we have shown selected examples of coordination networks including transition metals and azole building blocks. These materials display several potential applications, in gas or metallic

storage, molecular electronics, gas sensing, toxic metals sensing and capture, as well for medicinal applications. The development of nanoscale complexes, coordination polymers and metal-organic frameworks with azole based molecules is indeed flourishing and considered as an alternative to classic pyridine type networks to yield to diverse coordination networks with various topologies. Their suitable ligand field with Fe(II) along with their associated thermochromism observed for 1,2,4-triazole and tetrazole building blocks, make them often attractive to spin crossover developments toward nanodevices.[106] A number of other potential applications in various fields could also be proposed, be in opto-electronics, energy, public health and environmental issues. In particular, the biological properties of azole molecules constitute a potential functionality to explore within coordination networks, e.g., fungicide and pesticide properties known for 4R-1,2,4-triazole molecules.[24] This includes not only property testing but also the design of novel coordination networks including biomolecules and natural products. This development concerns metal-peptide networks,[107] as well as metal-biomolecule networks, e.g., with amino acids.[108] Despite the numerous derivatization possibilities offered by amino acids, due to the presence of several functional groups, their genuine chirality (except for glycine) and electronic asymmetry, can allow to introduce asymmetry in coordination network construction.[29] The synthesis of hybrid inorganic-organic materials containing azole based ligands, in particular in the form of nanoscale coordination polymers, is not to be neglected, given the unlimited potentialities offered by nanoparticles, opening a new world of investigation, particularly suitable in medicinal applications.[92]

Acknowledgments

Financial support from FNRS CDR 33694457 is gratefully acknowledged. We also acknowledge the input of all our collaborators cited in the reference section.

References

1. (a) Haasnoot, J. G. *Coord. Chem. Rev.* **2000**, *200–202*, 131–185; (b) Huang, Y.-Q.; Zhao, X.-Q.; Shi, W.; Liu, W.-Y.; Chen, Z.-L.; Cheng, P.; Liao, D.-Z.; Yan, S.-P. *Cryst. Growth Des.* **2008**, *8*, 3652–3660; (c) Deng, Y.; Liu, H.; Yu, B.; Yao, M. *Molecules* **2010**, *15*, 3478–3506; (d) Bai, S.-Q.; Young, D. J.; Andy Hor, T. S. *Chem. Asian J.* **2011**, *6*, 292; (e) Aromi, G.; Barrios, L. A.; Roubeau, O.; Gamez, P. *Coord. Chem. Rev.* **2011**, *255*, 485–546.
2. de Ruiter, G.; Lahav, M.; van der Boom, M. E. *Acc. Chem. Res.* **2014**, *47*, 3407–3416.
3. (a) Zhang, J.-P.; Zhang, Y.-B.; Lin, J.-B.; Chen, X.-M. *Chem. Rev.* **2012**, *112*, 1001; (b) Tăbăcaru, A.; Pettinari, C.; Galli, S. *Coord. Chem. Rev.* **2018**, *372*, 1–30.
4. Naik, A. D.; Dîrtu, M. M.; Leónard, A.; Tinant, B.; Marchand-Brynaert, J.; Su, B. L.; Garcia, Y. *Cryst. Growth Des.* **2010**, *10*, 1798–1807.

5. Lysenko, A. B.; Senchyk, G. A.; Domasevitch, K. V.; Hauser, J.; Fuhrmann, D.; Kobalz, M.; Krautscheid, H.; Neves, P.; Valente, A. A.; Goncalves, I. S. *Inorg. Chem.* **2015**, *54*, 8327–8338.
6. Meng, L.; Niu, Z.; Liang, C.; Dong, X.; Kang, L.; Li, G.; Li, C.; Han, Y.; Shi, Z.; Feng, S. *Chem. Eur. J.* **2018**, *24*, 13181–13187.
7. Wang, W.; Li, J.-L.; Jiang, C.; Hu, P.; Li, B.; Zhang, T.; Zhou, H.-C. *Chem. Commun.* **2018**, *54*, 13271–13274.
8. Boland, Y.; Tinant, B.; Safin, D. A.; Marchand-Brynaert, J.; Clérac, R.; Garcia, Y. *CrystEngComm* **2012**, *14*, 8153–8155.
9. Jafari, M.; Amani, V. *Sep. Sci. Plus* **2018**, *1*, 746–752.
10. Garcia, Y.; Adarsh, N. N.; Naik, A. D. *Chimia* **2013**, *67*, 411–418.
11. van Koningsbruggen, P. J.; Garcia, Y.; Kahn, O.; Fournès, L.; Kooijman, H.; Spek, A. L.; Haasnoot, J. G.; Moscovici, J.; Provost, K.; Michalowicz, A.; Renz, F.; Gütlich, P. *Inorg. Chem.* **2000**, *39*, 1891–1900.
12. (a) Garcia, Y.; Niel, V.; Munoz, M. C.; Real, J. A. *Top. Curr. Chem.* **2004**, *233*, 229–257; (b) Ksiazek, M.; Kusz, J.; Bialonska, A.; Bronisz, R.; Weselski, M. *Dalton Trans.* **2015**, *44*, 18563–18575; (c) Weselski, M.; Ksiazek, M.; Rokosz, D.; Dreczko, A.; Kusz, J.; Bronisz, R. *Chem. Commun.* **2018**, *54*, 3895–3898; (d) Ksiazek, M.; Weselski, M.; Ilczyszyn, M.; Kusz, J.; Bronisz, R. *Chem. Eur. J.* **2019**, *25*, 2250–2261; (e) Weselski, M.; Ksiazek, M.; Mess, P.; Kusz, J.; Bronisz, R. *Chem. Commun.* **2019**, *55*, 7033–7036.
13. Coronado, E.; Giménez-Marqués, M.; Mínguez Espallargas, G.; Rey, F.; Vitórica-Yrezábal, I. J. *J. Am. Chem. Soc.* **2013**, *135*, 15986–15989.
14. Roubeau, O. *Chem. Eur. J.* **2012**, *18*, 15230–15244.
15. Garcia, Y.; van Koningsbruggen, P. J.; Lapouyade, R.; Rabardel, L.; Kahn, O.; Wierczorek, M.; Bronisz, R.; Ciunik, Z.; Rudolf, M. F. *C. R. Acad. Sc. Paris Ser. IIc* **1998**, 523–532.
16. Lavrenova, L. G.; Shakirova, O. G.; Shvedenkov, Y. G.; Ikorskii, V. N.; Varnek, V. A.; Sheludyakova, L. A.; Larionov, S. V. *Koord. Khim.* **1999**, *25*, 208.
17. Dîrtu, M. M.; Rotaru, A.; Gillard, D.; Linares, J.; Codjovi, E.; Tinant, B.; Garcia, Y. *Inorg. Chem.* **2009**, *48*, 7838–7852.
18. Jureschi, C. M.; Linares, J.; Rotaru, A.; Ritti, M. H.; Parlier, M.; Dîrtu, M. M.; Wolff, M.; Garcia, Y. *Sensors* **2015**, *15*, 2388–2398.
19. Molnar, G.; Rat, S.; Salmon, L.; Nicolazzi, W.; Bousseksou, A. *Adv. Mater.* **2018**, *30*, 17003862.
20. Torres-Cavanillas, R.; Sanchis-Gual, R.; Dugay, J.; Coronado-Puchau, M.; Gimenez-Marques, M.; Coronado, E. *Adv. Mater.* **2019**, *31*, 1900039.
21. Zhao, T.; Cuignet, L.; Dîrtu, M. M.; Wolff, M.; Boldog, I.; Rotaru, A.; Garcia, Y.; Janiak, C. *J. Mater. Chem. C* **2015**, *3*, 7802–7812.
22. Vreugdenhil, W.; Van Diemen, J. H.; De Graaff, R. A. G.; Haasnoot, J. G.; Reedijk, J.; Van der Kraan, A. M.; Kahn, O.; Zarembowitch, J. *Polyhedron* **1990**, *9*, 2971–2979.
23. Garcia, Y.; Kahn, O.; Rabardel, L.; Chansou, B.; Salmon, L.; Tuchagues, J.-P. *Inorg. Chem.* **1999**, *38*, 4663–4670.
24. Bayer, H. O.; Cook, R. S.; Von Meyer, W. C. US Patent 382137628, 1974*Chem. Abstr.* **1972**, *76*, 113224.
25. Bartlett, R. K.; Humphrey, I. R. *J. Chem. Soc. C* **1967**, 1664.
26. Naik, A. D.; Marchand-Brynaert, J.; Garcia, Y. *Synthesis* **2008**, *1*, 149–154.
27. (a) Tahli, A.; MacLaren, J. K.; Boldog, I.; Janiak, C. *Inorg. Chim. Acta* **2011**, *374*, 506–513; (b) Gomez, V.; Lillo, V.; Escudero-Adan, E. C.; Martin, E.; Galan-Mascaros, J. R. *Dalton Trans.* **2013**, *42*, 6374–6380; (c) Kitchen, J. A.; Olguin, J.; Kulmaczewski, R.; White, N. G.; Milway, V. A.; Jameson, G. N. L.; Tallon, J. L.; Brooker, S. *Inorg. Chem.* **2013**, *52*, 11185–11199; (d) Chen, D.-M.; Ma, X.-Z.;

Zhang, X.-J.; Xu, N.; Cheng, P. *Inorg. Chem.* **2015**, *54*, 2976–2982; (e) Chen, D.-M.; Ma, J.-G.; Cheng, P. *Dalton Trans.* **2015**, *44*, 8926–8931; (f) Lin, J.-D.; Onet, C. I.; Schmitt, W. *Sci. Technol. Adv. Mater.* **2015**, *16*, 1–10; (g) Ye, Y.; Xiong, S.; Wu, X.; Zhang, L.; Li, Z.; Wang, L.; Ma, X.; Chen, Q.-H.; Zhang, Z.; Xiang, S. *Inorg. Chem.* **2016**, *55*, 292–299; (h) Chen, D.-M.; Tian, J.-Y.; Fang, S.-M.; Liu, C.-S. *CrystEngComm* **2016**, *18*, 2579–2584; (i) Chen, D.-M.; Tian, J.-Y.; Liu, C.-S. *Z. Anorg. Allg. Chem.* **2016**, *642*, 714–718; (j) Wang, L.; Ye, Y.; Li, Z.; Lin, Q.; Ouyang, J.; Liu, L.; Zhang, Z.; Xiang, S. *Cryst. Growth Des.* **2017**, *17*, 2081–2089; (k) Shao, M.; Li, M.-X.; Wang, Z.-X.; He, X.; Zhang, H.-H. *Cryst. Growth Des.* **2017**, *17*, 6281–6290; (l) Liu, M.; Yang, X.-F.; Zhu, H.-B.; Di, B.-S.; Zhao, Y. *Dalton Trans.* **2018**, *47*, 5245–5251; (m) Du, Y.; Su, H.; Fei, T.; Hu, B.; Zhang, J.; Li, S.; Pang, S.; Nie, F. *Cryst. Growth Des.* **2018**, *18*, 5896–5903.

28. (a) Naik, A. D.; Tinant, B.; Léonard, A.; Marchand-Brynaert, J.; Su, B. L.; Garcia, Y. *Cryst. Growth Des.* **2011**, *11*, 4034–4043; (b) Dîrtu, M. M.; Schmit, F.; Naik, A. D.; Rotaru, A.; Rusu, I.; Rackwitz, S.; Wolny, J. A.; Schünemann, V.; Garcia, Y. *Chem. Eur. J.* **2015**, *21*, 5843–5855; (c) Dîrtu, M. M.; Adarsh, N. N.; Naik, A. D.; Robeyns, K.; Garcia, Y. *New J. Chem.* **2016**, *40*, 9025–9029; (d) Dîrtu, M. M.; Naik, A. D.; Rotaru, A.; Spinu, L.; Poelman, D.; Garcia, Y. *Inorg. Chem.* **2016**, *55*, 4278–4295.
29. Naik, A. D.; Dîrtu, M. M.; Railliet, A. P.; Marchand-Brynaert, J.; Garcia, Y. *Polymer* **2011**, *3*, 1750.
30. Adarsh, N. N.; Dîrtu, M. M.; Naik, A. D.; Léonard, A. F.; Campagnol, N.; Robeyns, K.; Snauwaert, J.; Fransaer, J.; Su, B. L.; Garcia, Y. *Chem. Eur. J.* **2015**, *21*, 4300–4307.
31. Bati, A. S. R.; Yu, L.; Batmunkh, M.; Shapter, J. G. *Adv. Funct. Mater.* **2019**, *30*, 1902273.
32. Jiang, J.; Yu, J.; Corma, A. *Angew. Chem. Int. Ed.* **2010**, *49*, 3120–3145.
33. Su, B. L.; Garcia, Y. *Eur. J. Inorg. Chem.* **2019**, *27*, 3123–3125.
34. (a) Tezer, H.; Erkocoglu, M.; Kara, A.; Bayakci, B.; Düzova, A.; Teksam, O.; Aysun, S. *Eur. J. Pediatr.* **2011**, *170*, 397; (b) EPA *EPA Fact Sheet. EPA-823-F-01-011*. EPA, Office of Water: Washington, DC, 2001.
35. (a) Beurroies, I.; Boulhout, M.; Llewellyn, P. L.; Kuchta, B.; Férey, G.; Serre, S.; Denoyel, R. *Angew. Chem. Int. Ed.* **2010**, *49*, 7526–7529; (b) Neimark, A. V.; Coudert, F. X.; Triguero, C.; Boutin, A.; Fuchs, A. H.; Beurroies, I.; Denoyel, R. *Langmuir* **2011**, *27*, 4734–4741.
36. Radi, S.; Toubi, Y.; Bacquet, M.; Degoutin, S.; Mabkhot, Y. N.; Garcia, Y. *RSC Adv.* **2016**, *6*, 34212.
37. (a) Radi, S.; Tighadouini, S.; Bacquet, M.; Degoutin, S.; Garcia, Y. *Anal. Methods* **2016**, *8*, 6923–6931; (b) El Massaoudi, M.; Radi, S.; Bacquet, M.; Degoutin, S.; Adarsh, N. N.; Robeyns, K.; Garcia, Y. *Inorg. Chem. Front.* **2017**, *4*, 1821; (c) Tighadouini, S.; Radi, S.; Anannaz, M.; Bacquet, M.; Degoutin, S.; Tillard, M.; Eddike, D.; Amhamdi, H.; Garcia, Y. *New J. Chem.* **2018**, *42*, 13229–13240; (d) El Massaoudi, M.; Radi, S.; Bacquet, M.; Degoutin, S.; Garcia, Y. *J. Environ. Chem. Eng.* **2018**, *6*, 5980–5989; (e) Tighadouini, S.; Radi, S.; Elidrissi, A.; Haboubi, K.; Bacquet, M.; Degoutin, S.; Zaghrioui, M.; Garcia, Y. *Beilstein J. Nanotechnol.* **2019**, *10*, 262–273; (f) Tighadouini, S.; Radi, S.; Ferbinteanu, M.; Garcia, Y. *ACS Omega* **2019**, *4*, 3954–3964; (g) Tighadouini, S.; Radi, S.; Elidrissi, A.; Zaghrioui, M.; Garcia, Y. *Eur. J. Inorg. Chem.* **2019**, *27*, 3180–3186; (h) Tighadouini, S.; Radi, S.; Garcia, Y. *Mol. Syst. Des. Eng.* **2020**, https://doi.org/10.1039/C9ME00140A.
38. (a) Adarsh, N. N.; Dîrtu, M. M.; Guionneau, P.; Devlin, E.; Sanakis, Y.; Howard, J. A. K.; Chattopadhyay, B.; Garcia, Y. *Eur. J. Inorg. Chem.* **2019**, *5*,

585–591; (b) Yang, Z.-J.; Ni, T.-J.; He, G.-J.; Huang, Q.-Q.; Yuan, Q.-T.; Zheng, W.-Q. *Asian J. Chem.* **2015**, *27*, 4103–4105.
39. Quesada, M.; Prins, F.; Bill, E.; Kooijman, H.; Gamez, P.; Roubeau, O.; Spek, A. L.; Haasnoot, J. G.; Reedijk, J. *Chem. Eur. J.* **2008**, *14*, 8486–8499.
40. Drabent, K.; Bronisz, R.; Ruldolf, M. F. *Conf. Proc. ICAME* **1995**, *50*, 7.
41. Bronisz, R.; PhD thesis, University of Wroclaw, Poland, 1999.
42. Suarez-Garcia, S.; Adarsh, N. N.; Molnar, G.; Bousseksou, A.; Garcia, Y.; Dîrtu, M. M.; Saiz-Poseu, J.; Robles, R.; Ordejon, P.; Ruiz-Molina, D. *ACS Appl. Nano Mater.* **2018**, *1*, 2662–2668.
43. Adarsh, N. N.; Dîrtu, M. M.; Rotaru, A.; Garcia, Y. *Hyperfine Interact.* **2017**, *238*, 60.
44. Coronado, E. *Nat. Rev. Mater.* **2020**, *5*, 87–104.
45. Zhang, L.; August, D.; Zhong, J.; Whitehead, G. F. S.; Vitorica-Yrezabal, I. J.; Leigh, D. A. *J. Am. Chem. Soc.* **2018**, *140*, 4982–4985.
46. Jin, C. M.; Zhu, Z.; Chen, Z. F.; Hu, Y. J.; Meng, X. G. *Cryst. Growth Des.* **2010**, *10*, 2054–2056.
47. Liu, X. G.; Wang, L. Y.; Zhu, X.; Li, B. L.; Zhang, Y. *Cryst. Growth Des.* **2009**, *9*, 3997–4005.
48. Soudry, H.; Desmarets, C.; Gontard, G.; Edgington, T.; Cooksy, A. L.; Amouri, H. *Dalton Trans.* **2017**, *46*, 10240–10245.
49. Robinson, W. R. *J. Chem. Ed.* **1985**, *62*, 1001.
50. Nierlich, M.; Charpin, P.; Herpin, P. *C. R. Acad. Sci.* **1973**, *276*, 1–3.
51. van Albada, G. A.; van der Horst, M. G.; Mutikainen, I.; Turpeinen, U.; Reedijk, J. *J. Chem. Cryst.* **2008**, *38*, 519–523.
52. Varonka, M. S.; Warren, T. H. *Inorg. Chem.* **2009**, *48*, 5605–5607.
53. Döring, A.; Flörke, U.; Hoffmann, A.; Jones, M. D.; Kuckling, D.; de Vasconcellos, J. M.; Herres-Pawlis, S. *Z. Anorg. Allg. Chem.* **2015**, *641*, 2147–2156.
54. Vantomme, G.; Jiang, S.; Lehn, J.-M. *J. Am. Chem. Soc.* **2014**, *136*, 9509–9518.
55. Żurowska, B.; Ślepokura, K.; Fabijańska, M.; Ochocki, J. *Inorg. Chim. Acta* **2013**, *407*, 19–24.
56. Tomat, E.; Cuesta, L.; Lynch, V. M.; Sessler, J. L. *Inorg. Chem.* **2007**, *46*, 6224–6226.
57. Mercer, D. J.; Loeb, S. J. *Dalton Trans.* **2011**, *40*, 6385–6387.
58. Hutchinson, D. J.; Hanton, L. R.; Moratti, S. C. *Inorg. Chem.* **2013**, *52*, 2716–2728.
59. Hutchinson, D. J.; Hanton, L. R.; Moratti, S. C. *Inorg. Chem.* **2011**, *50*, 7637–7649.
60. Gobeze, W. A.; Milway, V. A.; Moubaraki, B.; Murray, K. S.; Brooker, S. *Dalton Trans.* **2012**, *41*, 9708–9721.
61. Szymczak, N. K.; Berben, L. A.; Peters, J. C. *Chem. Commun.* **2009**, 6729.
62. Browne, C.; Ramsay, W. J.; Ronson, T. K.; Medley-Hallam, J.; Nitschke, J. R. *Angew. Chem. Int. Ed.* **2015**, *54*, 11122–11127.
63. Cao, X.-Y.; Harrowfield, J.; Nitschke, J.; Ramírez, J.; Stadler, A.-M.; Kyritsakas-Gruber, N.; Madalan, A.; Rissanen, K.; Russo, L.; Vaughan, G.; Lehn, J.-M. *Eur. J. Inorg. Chem.* **2007**, 2944–2965.
64. El Massaoudi, M.; Radi, S.; Salhi, A.; Mabkhot, Y. N.; Al Showiman, S. S.; Ghabbour, H. A.; Adarsh, N. N.; Garcia, Y. *New J. Chem.* **2018**, *42*, 11324–11333.
65. Baryshnikov, G.; Minaev, B.; Korop, A.; Minaeva, V.; Gusev, A. *Russ. J. Inorg. Chem.* **2013**, *58*, 928–934.
66. Minaeva, V.; Minaev, B.; Baryshnikov, G.; Kopylova, T.; Gadirov, R.; Eremina, N. *Russ. J. Gen. Chem.* **2011**, *81*, 2332–2344.
67. Naik, A. D.; Beck, J.; Dîrtu, M. M.; Bebrone, C.; Tinant, B.; Robeyns, K.; Marchand-Brynaert, J.; Garcia, Y. *Inorg. Chim. Acta* **2011**, *368*, 21–28.
68. Govor, E. V.; Lysenko, A. B.; Rusanov, E. B.; Chernega, A. N.; Krautscheid, H.; Domasevitch, K. V. *Z. Anorg. Allg. Chem.* **2010**, *636*, 209–217.

69. Senchyk, G. A.; Lysenko, A. B.; Rusanov, E. B.; Chernega, A. N.; Krautscheid, H.; Domasevitch, K. V. *Inorg. Chim. Acta* **2009**, *362*, 4439–4448.
70. Miao, S.; Ji, B.; Zhou, L. *Russ. J. Coord. Chem.* **2015**, *41*, 339–344.
71. Deligne, N.; Gonze, V.; Bayot, D.; Devillers, M. *Eur. J. Inorg. Chem.* **2008**, 896–902.
72. Yang, L.; Powell, D. R.; Houser, R. P. *Dalton Trans.* **2007**, 955–964.
73. Wang, N.; Chao Feng, Y.-C.; Shi, W.; Zhao, B.; Cheng, P.; Liao, D.-Z.; Yana, S.-P. *CrystEngComm* **2012**, *14*, 2769–2778.
74. Benaissa, H.; Wolff, M.; Robeyns, K.; Van Hecke, K.; Knör, G.; Campagnol, N.; Fransaer, J.; Garcia, Y. *Cryst. Growth Des.* **2019**, *19*, 5292–5307.
75. (a) Campagnol, N.; Souza, E. R.; De Vos, D. E.; Binnemans, K.; Fransaer, J. *Chem. Commun.* **2014**, *50*, 12545–12547; (b) Campagnol, N.; Van Assche, T. R. C.; Li, M.; Stappers, L.; Dinca, M.; Denayer, J. F. M.; Binnemans, K.; De Vos, D. E.; Fransaer, J. *J. Mater. Chem. A.* **2016**, *4*, 3914–3925; (c) Van Assche, T. R. C.; Campagnol, N.; Muselle, T.; Terryn, H.; Fransaer, J.; Denayer, J. F. M. *Microporous Mesoporous Mater.* **2016**, *224*, 302–310.
76. Fischer, N.; Iszak, D.; Klapötke, T. M.; Stierstorfer, J. *Chem. Eur. J.* **2013**, *19*, 8948.
77. Fischer, N.; Klapötke, T. M.; Peeters, K.; Rusan, M.; Stierstorfer, J. *Z. Anorg. Allg. Chem.* **2011**, *637*, 1693.
78. Naik, A. D.; Robeyns, K.; Meunier, C. F.; Léonard, A. F.; Rotaru, A.; Tinant, B.; Filinchuk, Y.; Su, B. L.; Garcia, Y. *Inorg. Chem.* **2014**, *53*, 1263–1265.
79. Safin, D. A.; Railliet, A. P.; Robeyns, K.; Mitoraj, M.; Kubisiak, P.; Sagan, F.; Garcia, Y. *New J. Chem.* **2017**, *41*, 6210.
80. Guo, Y.; Xue, S.; Dîrtu, M. M.; Garcia, Y. *J. Mater. Chem. C* **2018**, *6*, 3895–3900.
81. (a) Garcia, Y.; van Koningsbruggen, P. J.; Codjovi, E.; Lapouyade, R.; Kahn, O.; Rabardel, L. *J. Mater. Chem.* **1997**, *7*, 857–858; (b) van Koningsbruggen, P. J.; Garcia, Y.; Codjovi, E.; Lapouyade, R.; Kahn, O.; Fournès, L.; Rabardel, L. *J. Mater. Chem.* **1997**, *7*, 2069–2075.
82. Rodriguez-Jimenes, S.; Felthon, H. L. C.; Brooker, S. *Angew. Chem. Int. Ed.* **2016**, *55*, 15067–15071.
83. Wenger, O. S. *Chem. Rev.* **2013**, *113*, 3686–3733.
84. (a) Novio, F.; Simmchen, J.; Vázquez-Mera, N.; Amorín-Ferré, L.; Ruiz-Molina, D. *Coord. Chem. Rev.* **2013**, *257*, 2839–2847; (b) Della Rocca, J.; Liu, D.; Lin, W. *Acc. Chem. Res.* **2011**, *44*, 957–968.
85. Mu, J.; He, L.; Huang, P.; Chen, X. *Coord. Chem. Rev.* **2019**, *399*, 213039.
86. Lin, W. *Chem. Rev.* **2015**, *115*, 10407–10409.
87. He, C.; Liu, D.; Lin, W. *Chem. Rev.* **2015**, *115*, 11079–11108.
88. Zhao, H.; Xu, J.; Li, Y.; Guan, X.; Han, X.; Xu, Y.; Zhou, H.; Peng, R.; Wang, J.; Liu, Z. *ACS Nano* **2019**, *13*, 13127–13135.
89. (a) Deka, H.; Kumar, A.; Patra, S.; Awasthi, M. K.; Singh, S. K. *Dalton Trans.* **2020**, *49*, 757–763; (b) Solórzano, R.; Tort, O.; García-Pardo, J.; Escribà, T.; Lorenzo, J.; Arnedo, M.; Ruiz-Molina, D.; Alibés, R.; Busqué, F.; Novio, F. *Biomater. Sci.* **2019**, *7*, 178–186; (c) Novio, F.; Lorenzo, J.; Nador, F.; Wnuk, K.; Ruiz-Molina, D. *Chem. Eur. J.* **2014**, *20*, 15443–15450; (d) Amorín-Ferré, L.; Busqué, F.; Bourdelande, J. L.; Ruiz-Molina, D.; Hernando, J. *Chem. Eur. J.* **2013**, *19*, 17508–17516.
90. Adarsh, N. N.; Novio, F.; Ruiz-Molina, D. *Dalton Trans.* **2016**, *45*, 11233–11255.
91. Nador, F.; Wnuk, K.; García-Pardo, J.; Lorenzo, J.; Solorzano, R.; Ruiz-Molina, D.; Novio, F. *ChemNanoMat* **2018**, *4*, 183–193.
92. Suárez-García, S.; Arias-Ramos, N.; Frias, C.; Candiota, A. P.; Arús, C.; Lorenzo, J.; Ruiz-Molina, D.; Novio, F. *ACS Applied Materials Interf.* **2018**, *10*, 38819–38832.
93. Adarsh, N. N.; Frias, C.; Ponnoth Lohidakshan, T. M.; Lorenzo, J.; Novio, F.; Garcia-Pardo, J.; Ruiz-Molina, D. *Chem. Eng. J.* **2018**, *340*, 94–102.

94. Karrouchi, K.; Yousfi, E.; Sebbar, N. K.; Ramli, Y.; Taoufik, J.; Ouzidan, Y.; Ansar, M.; Mabkhot, Y. N.; Ghabbour, H. A.; Radi, S. *Int. J. Mol. Sci.* **2017**, *18*, 2215.
95. Karrouchi, K.; Radi, S.; Ramli, Y.; Taoufik, J.; Mabkhot, Y. N.; Al-aizari, F. A.; Ansar, M. *Molecules* **2018**, *23*, 134.
96. Pillai, R. R.; Karrouchi, K.; Fettach, S.; Armaković, S.; Armaković, S. J.; Brik, Y.; Taoufik, J.; Radi, S.; Faouzi, M. E.; Ansar, M. H. *J. Mol. Struct.* **2019**, *1177*, 47–54.
97. Reddy, T. S.; Kulhari, H.; Reddy, V. G.; Bansal, V.; Kamal, A.; Shukla, R. *Eur. J. Med. Chem.* **2015**, *101*, 790–805.
98. Devereux, M.; O'Shea, D.; O'Connor, H.; Grehan, H.; Connor, G.; McCann, M.; Rosair, G.; Lyng, F.; Kellett, A.; Walsh, M.; Egan, D.; Thati, B. *Polyhedron* **2007**, *26*, 4073–4084.
99. Bouchouit, M.; Said, M. E.; Kara Ali, M.; Bouacida, S.; Merazig, H.; Kacem, H.; Chaouche, H.; Chibani, A.; Zouchoune, B.; Belfaitah, A.; Bouraiou, A. *Polyhedron* **2016**, *119*, 248–259.
100. Tabassum, S.; Asim, A.; Arjmand, F.; Afzal, M.; Bagchi, V. *Eur. J. Med. Chem.* **2012**, *58*, 308–316.
101. Li, M. X.; Zhang, L. Z.; Chen, C. L.; Niu, J. Y.; Ji, B. S. *J. Inorg. Biochem.* **2012**, *106*, 117–125.
102. Dholakiya, P. P.; Patel, M. N. *Synth. React. Inorg. Met.-Org. Chem.* **2004**, *34*, 383–395.
103. Chkirate, K.; Fettach, S.; Karrouchi, K.; Sebbar, N. K.; El Essasi, M.; Mague, J. T.; Radi, S.; El Faouzi, A. M.; Adarsh, N. N.; Garcia, Y. *J. Inorg. Biochem.* **2019**, *191*, 21–28.
104. Chkirate, K.; Karrouchi, K.; Dege, N.; Sebbar, N. K.; Ejjoummany, A.; Radi, S.; Adarsh, N. N.; Talbaoui, A.; Ferbinteanu, M.; El Essasi, M.; Garcia, Y. *New J. Chem.* **2020**, *44*, 2210–2221.
105. Hu, S.; Mac, C.; Zhan, F.; Cao, Y.; Hu, P.; Zhen, Q. *Chem. Pap.* **2017**, *71*, 1323–1329.
106. Sawczak, M.; Jendrzejewski, R.; Maskowicz, D.; Garcia, Y.; Gosh, A. C.; Gazda, M.; Czechowski, J.; Śliwiński, G. *Eur. J. Inorg. Chem.* **2019**, *27*, 3249–3255.
107. Rabone, J.; Yue, Y. F.; Chong, S. Y.; Stylianou, K. C.; Bacsa, J.; Bradshaw, D.; Darling, G. R.; Berry, N. G.; Khimyak, Y. Z.; Ganin, A. Y.; Wiper, P.; Claridge, J. B.; Rosseinsky, M. J. *Science* **2010**, *329*, 1053–1057.
108. Joarder, B.; Chaudhari, A. K.; Nagarkar, S. S.; Manna, B.; Ghosh, S. K. *Chem. Eur. J.* **2013**, *19*, 11178–11183.